High fluxes of deep volatiles from ocean island volcanoes: Insights from El Hierro, Canary Islands

Z. Taracsák[a,*], M.E. Hartley[a], R. Burgess[a], M. Edmonds[b], F. Iddon[b], M-A. Longpré[c]

[a]*School of Earth and Environmental Sciences, University of Manchester, M13 9PL, United Kingdom*
[b]*Department of Earth Sciences, University of Cambridge, Downing Street, Cambridge CB2 3EQ, United Kingdom*
[c]*School of Earth and Environmental Sciences, Queens College, City University of New York, Flushing, NY 11367, USA*

Abstract

Basaltic volcanism contributes significant fluxes of volatiles (CO_2, H_2O, S, F, Cl) to the Earth's surface environment. Quantifying volatile fluxes requires initial melt volatile concentrations to be determined, which can be accessed through crystal-hosted melt inclusions. However, melt inclusions in volatile-rich mafic alkaline basalts, such as those erupted at ocean islands, often trap partially degassed melts, meaning that magmatic volatile fluxes from these tectonic settings are often significantly underestimated. We have measured major, trace element and volatile concentrations in melt inclusions from a series of young (<20 ka) basanites from El Hierro, Canary Islands. Our melt inclusions show some of the highest CO_2 (up to 3600 ppm) and S (up to 4290 ppm) concentrations measured in ocean island basalts to date, in agreement with data from the recent 2011-2012 eruption. Volatile enrichment is observed in melt inclusions with crystallisation-controlled major element compositions and highly variable trace element ratios such as La/Yb. We use volatile-trace element ratios to calculate original magmatic CO_2 contents up to 4.2 wt%, which indicates at least 65% of the original CO_2 was degassed prior to melt inclusion

*Corresponding author
Email address: zoltan.taracsak@manchester.ac.uk (Z. Taracsák)

trapping. The trace element contents and ratios of El Hierro magmas are best reproduced by 1-8% partial melting of a garnet lherzolite mantle source. Our projected CO_2 (200-680 ppm) and S (265-450 ppm) concentrations for the source are consistent with upper estimates for primitive mantle. However, El Hierro magmas have elevated F/Nd and F/Cl in comparison with melts from a primitive mantle, indicating that the mantle must also contain a component enriched in F and other volatiles, most probably recycled oceanic lithosphere.

Our modelled original magmatic CO_2 contents indicates that, per mass unit, volatile fluxes from El Hierro magmas are up to two orders of magnitude greater than from typical mid-ocean ridge basalts and 1.5 to 7 times greater than from recent Icelandic eruptions, indicating large variability in the primary volatile content of magmas formed in different geodynamic settings, or even within different ocean islands. Our results highlight the importance of characterising mantle heterogeneity in order to accurately constrain both short- and long-term magmatic volatile emissions and fluxes from ocean island volcanoes.
Keywords:
melt inclusions, volatiles, CO_2 degassing, volatile recycling, El Hierro, Canary Islands

1. Introduction

Volatiles (H_2O, CO_2, F, S, Cl) often constitute just a few weight percent of silicate melts, yet they impact a variety of processes in magmatic systems. In particular, volatiles strongly influence melt generation processes through changing the melting depth and degree of the source mantle (e.g. Dasgupta et al., 2007; Green et al., 2010), and also affect the order in which crystallising phases appear on the liquidus (e.g. Gaetani et al., 1993; Métrich and Rutherford, 1998).

The volatile-carrying capacity of a magma is strongly influenced by its major element composition (e.g. Dixon, 1997). Mid-ocean ridge basalts (MORB) constitute ~75% of

the Earth's annual magmatic output (Schmincke, 2004) and typically contain <0.3 wt% total volatiles (Saal et al., 2002). Ocean islands basalts (OIB) represent just ~10% of erupted magmas, but as they can contain >5 wt% volatiles (Dixon et al., 1997) likely contribute disproportionately more to global volcanic gas emissions. Volatile enrichment is most prominent in trace element and radiogenic isotope-enriched (e.g. HIMU) OIBs (Cabral et al., 2014; Boudoire et al., 2018). A good understanding of the origin, storage and flux of volatiles from OIB magmas is crucial if we are to provide reasonable estimates of volcanic volatile fluxes into the environment (Burton et al., 2013).

Determining magmatic volatile contents is complicated by their low solubility in silicate melts at low pressures, with melt volatile contents being reduced by degassing as they ascend towards the surface. Formation of immiscible sulfide globules at high melt sulfur concentrations can also lower the melt sulfur content. These issues can be circumvented by measuring volatile contents in crystal-hosted melt inclusions (MIs), which are theoretically shielded from processes like crystallization or shallow degassing from their carrier melt (e.g. Métrich and Wallace, 2008; Koleszar et al., 2009; Edmonds et al., 2013; Hartley et al., 2014; Cabral et al., 2014; Wallace et al., 2015). In practice, MI compositions are modified by post-entrapment crystallisation, diffusive re-equilibration with their external carrier melt, and sulfide formation due to melt reduction (Danyushevsky et al., 2002; Gaetani et al., 2012). These processes can often be corrected to establish original inclusion compositions (Danyushevsky et al., 2000; Danyushevsky and Plechov, 2011).

This work focuses on El Hierro in the Canary Islands, a location relatively understudied until the occurrence of a submarine eruption 2 km off the southern tip of the island, between October 2011 and March 2012. The eruption received significant attention from geoscientists due to abundant surface gas measurements and seismic data recorded pre-, syn- and post-eruption (López et al., 2012; Pérez et al., 2012; Melián et al., 2014; Klügel et al., 2015). Floating rocks collected from the ocean during the eruption enabled petro-

logical studies of the magmatic plumbing system to infer the origin of the magma feeding the eruption (Troll et al., 2012; Martí et al., 2013a; Sigmarsson et al., 2013; Longpré et al., 2014). Volatile contents of MIs reveal that the erupted magma was one of the most CO_2- and S-enriched oceanic island basalts known to date. The estimated minimum volatile budget of the eruption is 1.3–2.1 Tg CO_2 and 1.8–2.9 Tg S (Longpré et al., 2017). However, it remains an outstanding question whether El Hierro magmas have been characterised by similar volatile enrichment over the past 20 ka.

Here we present major, trace and volatile element data from olivine- and clinopyroxene-hosted MIs from young (<20 ka) tephra samples collected from multiple locations on El Hierro. Melt inclusion compositions are discussed with an emphasis on melt genesis and evolution. Trace element data are used to identify mantle source characteristics, while volatiles combined with volatile and lithophile trace element ratios are utilised to estimate original magmatic volatile contents and the timing of their exsolution. The origin of volatile element enrichment in El Hierro magmas is also explored in detail. In this work, we highlight the importance of volatile-rich magmas erupting on ocean islands to both the global and local environment, and compare the volatile content of El Hierro magmas with other magmatic systems.

2. Geological Background

The Canary Archipelago comprises seven volcanic islands (Fig. 1A) formed above >80 km- Jurassic oceanic lithosphere. The easternmost islands have been active since the early Neogene (Coello et al., 1992; Hoernle and Schmincke, 1993), with some submarine rocks dated to the late Cretaceous (Le Bas et al., 1986; Balogh et al., 1999). The Canary Islands are characterised by low magma supply rate and relatively low eruption frequency: 13 eruptions have occurred over four islands since 1500 CE, 10 of these on La Palma or Tenerife (Fig. 1A). Seismic tomography indicates low-velocity anomalies down to the

core-mantle boundary beneath the archipelago, which have been interpreted as evidence for a deep mantle plume in the region (French and Romanowicz, 2015). Published Sr-Nd-Pb, O, He and Os isotopic data suggest a heterogeneous mantle source that includes a component of recycled oceanic lithosphere (e.g. Lundstrom et al., 2003; Day et al., 2010; Day and Hilton, 2011).

El Hierro is the youngest island in the Canary Archipelago; its oldest subaerial volcanics have been dated at 1.11 Ma (Guillou et al., 1996). It is built up by three successive subaerial volcanoes: the Tiñor volcano, the El Golfo volcano, and the Rift Volcanics, which post-date the collapse of the El Golfo volcano (Carracedo et al., 2001) (Fig. 1). Volcanism on El Hierro is dominated by mafic alkaline magmas. Petrological and geophysical studies of the 2011-2012 eruption suggest a vertically extensive magma plumbing system ranging from 10 to 30 km (Stroncik et al., 2009; López et al., 2012; Longpré et al., 2014; Klügel et al., 2015). Clinopyroxene-melt thermobarometry in young ankaramites and some dredged basanites around the island indicate crystallization pressures of 400-1000 MPa, extending into the upper mantle (Stroncik et al., 2009; Longpré, 2009).

3. Samples, analytical techniques and data processing

Our samples comprise glassy tephras collected from El Hierro pyroclastic deposits that post-date the last glacial maximum (Fig. 1B). The seven sampling locations cover all three rift systems on the island. Two samples were collected from Tanganasoga, a large edifice near the centre of El Hierro. From the western rift system we collected samples from scoria cones next to the village of Sabinosa and at Montañita Negra. From the southern rift system we collected samples from the Mercade and Montañas de Julán scoria cones, and from the eastern rift we collected one sample from a scoria cone near the village of Tamaduste. Tephra clasts were hand-crushed in a stainless steel mortar, and olivine crystals containing glassy melt inclusions were picked from sieved size fractions between 0.25 and 2 mm.

Olivines were individually ground to expose MIs, then mounted in epoxy and polished for analysis. Clinopyroxene megacrysts >10 mm in length, collected near the summit of Tanganasoga, were cut, mounted in epoxy and polished to expose MIs. Inclusions were typically ellipsoidal in shape, with diameters between 14 and 714 μm (mean diameter 117 μm). Bubbles were observed in 47 MIs (52%) and occupy between 0.3 and 59.2 vol% of the inclusion (Fig. S6). Several inclusions contained crystals, generally Fe-Ti oxides, together with the glass and bubble. Four analysed inclusions from Tanganasoga contained a sulfide globule ~2-10 μm in diameter. Sulfides were not observed in the groundmass material. Small (<10 μm) fluid inclusions were present in some olivines.

Trace and volatile (H_2O, CO_2, F and Cl) element concentrations in a total of 80 olivine-hosted MIs, 10 clinopyroxene-hosted MIs, and 16 tephra glasses and embayments along crystal rims, were measured by secondary ion mass spectrometry (SIMS) using the CAMECA IMS-4f instrument at the University of Edinburgh. The C and H measurements were calibrated by repeat analyses of basaltic glass standards (Shishkina et al., 2010) (Fig. S2). The precision of carbon measurements was better than ±10% (1σ) at concentrations ≤500 ppm, and ±7% at concentrations >500 ppm. The precision of H_2O measurements was ±3-6%. Precision and accuracy of trace element measurements were monitored by repeat analyses of glass standards. Precision was ±1-5% (1σ) for trace elements in higher abundance (Ba, Zr, Nb, Y, La), and ±10-20% for trace elements in low abundance (Dy, Yb, Lu). Following SIMS analyses, glasses and minerals were analysed for their major, minor elements and volatiles S and Cl by electron microprobe (EPMA) using the CAMECA SX100 instrument at the University of Manchester. Fluorine concentrations in five MIs were measured by EPMA at the University of Cambridge to verify the SIMS fluorine data. Compositional data and details of all analytical methods are provided as supplementary material.

Inclusion-hosted bubbles were analysed by micro-Raman spectroscopy using a Ren-

ishaw inVia instrument at the University of Manchester. Spectra were acquired using a 514 nm laser at 50% power, with acquisition time 10 s over 10 accumulations. Of the 41 inclusion-hosted bubbles analysed, 27 bubbles in samples from Tanganasoga, Tamaduste or Sabinosa contained detectable CO_2. Raman spectra were processed by fitting Gaussian distributions to the Fermi diad peaks. Fitted peak positions were then used to determine the separation of the Fermi diad, which is proportional to the CO_2 fluid density. The CO_2 density was calculated using the calibration of Wang et al. (2011). Bubble CO_2 contents were obtained through mass balance calculations following the method of Steele-Macinnis et al. (2011) and using a melt density of 2750 kg/m^2. The CO_2-bearing bubbles occupied $\leq$11 vol% of their host inclusions.

4. Results

4.1. Major Elements

Measured melt inclusion compositions lie between 38.6-52.9 wt% SiO_2, 2.2-6.4 wt% MgO, 1.9-5.6 wt% Na_2O and 8.3-15.1 wt% $FeO_{(t)}$ (data are available as supplementary material). However, olivine-hosted MIs experience both post-entrapment crystallization (PEC) and diffusive Fe loss during cooling. Published whole-rock and glass SiO_2 and FeO contents from El Hierro are linearly correlated (R^2=0.938), yet measured inclusion compositions show Fe depletion up to 2 wt% relative to the FeO-SiO_2 correlation, indicative of diffusive Fe loss (Longpré et al., 2014). We used Petrolog3 (Danyushevsky and Plechov, 2011) to correct MIs for PEC and diffusive Fe loss. Calculations were performed using the olivine-melt equilibrium model of Putirka (2005) and Fe^{3+}/Fe^{2+} = 0.35, as calculated for the 2011-2012 erupted products using ilmenite-magnetite oxybarometry (Longpré et al., 2014, 2017). PEC corrections between 0 and 18.3% were required to restore inclusion compositions to equilibrium with their host olivine. The average PEC

correction was 4.3%. Five olivine-hosted MIs required a PEC correction >10%. For 8 inclusions Petrolog3 predicts negative PEC values, i.e. olivine addition to the inclusion. The amount of olivine addition predicted is always <4.2%, and typically <2%, which is small in comparison to the Fe-loss correction for these inclusions. Following the PEC and Fe-loss corrections, trace element and volatile concentrations were corrected using the distribution coefficients listed in the supplementary material.

For clinopyroxene-hosted MIs, the measured Mg# of the host was generally lower than the Mg# of clinopyroxene calculated to be in equilibrium with the inclusion using $Kd_{cpx-liq}^{Mg-Fe}$=0.28 (Putirka, 2008). Haloes surrounding the MIs were not observed in back-scattered electron images, ruling out any PEC on the inclusion walls. Clinopyroxene-hosted inclusions were therefore only corrected for diffusive Fe loss.

Following PEC and Fe-loss corrections, the olivine- and clinopyroxene-hosted MIs contain 37.8-53.5 wt% SiO_2, 2.3-9.2 wt% MgO, and 8.3-15.5 wt% $FeO_{(t)}$ (Fig. 3).

4.2. Trace elements

Trace element concentrations in MIs generally fall within the range of published whole-rock compositions for El Hierro lavas (Fig. 4A) (Carracedo et al., 2001; Longpré, 2009; Day et al., 2010; Martí et al., 2013b). Concentrations of incompatible lithophile elements (ILE) such as Zr increase with decreasing MgO content (Fig. 4B). Trace element ratios cover a much wider range than previously published whole-rock and MI data: La/Yb varies between 5 and 70, and variation is high even within hosts with a narrow Mg# range (Fig. 4C). Inclusions from the Tanganasoga ankaramite hosted in Fo_{78-79} olivines have La/Yb between 15 and 58; this La/Yb variation is three times larger than measured in MIs from the 2011-2012 eruption (Longpré et al., 2017). Similarly large variations in La/Yb are observed in other samples, especially those from eruption centres along the southern rift. Melt inclusions from the western rift zone are characterised by lower La/Yb between

5-27. Primitive MIs hosted in Fo>82 olivines have the most ILE-depleted compositions.

In addition to olivine-hosted MIs, we analysed 10 clinopyroxene-hosted MIs from Tanganasoga. We observe no systematic differences in the major and trace element concentrations of olivine- and clinopyroxene-hosted inclusions, although trace element ratios in clinopyroxene-hosted MIs are somewhat less variable, with 27<La/Yb<35. The small number of clinopyroxene-hosted MIs precludes statistical comparison with olivine-hosted MI, and any observed compositional differences might not persist if more clinopyroxene-hosted MIs were to be measured.

4.3. Volatiles

The studied inclusions have maximum glass CO_2 and S contents of 3610 ppm and 4290 ppm, respectively (Fig. 5). Most MIs from Tanganasoga contain >3000 ppm S. The matrix glasses contain 0-55 ppm CO_2 and 140-500 ppm S (expect for one glass analyses with 1890 ppm S). H_2O concentrations vary between 0.06-2.22 wt% for MIs and 0.07-0.38 wt% for matrix glasses. Melt inclusions contain 970-3350 ppm F and 290-1500 ppm Cl. One MI has an anomalously high Cl content of 2450 ppm. Matrix glasses contain 1520-3220 ppm F and 380-1340 ppm Cl (Fig. S5).

Of the 27 MIs containing detectable CO_2 in inclusion-hosted bubbles, nine were also analysed by SIMS. For these inclusions, it is possible to determine their total CO_2 by summing the glass and bubble CO_2 contents. The highest bubble CO_2 contents of 0.83-1.02 wt% were measured in MIs from Tanganasoga ankaramite samples; these inclusions also had the largest bubbles occupying 7.4-10.5 vol% of the inclusion. Inclusions with bubble proportions >10% likely formed due to heterogeneous trapping of melt and fluid phases, such that their total inclusion CO_2 overestimates the true CO_2 content of the trapped melt (Moore et al., 2015; Steele-MacInnis et al., 2017). The two MIs with the largest bubble proportions have diameters <40 μm. If these MI radii are uncertain by just 10%, their

calculated bubble could be reduced to 5.8-7.7 vol%, which in turn decreases their calculated total CO_2 contents by several thousand ppm. Estimation of true MI glass volumes is further complicated by the presence of included oxides. If MIs with bubbles <10 vol% are considered to represent homogeneously trapped melts, then up to 85% of the total inclusion CO_2 may be sequestered into the bubble. This is consistent with previous studies demonstrating that inclusion-hosted bubbles can sequester up to 90% of an inclusion's original CO_2 (Hartley et al., 2014; Wallace et al., 2015). Our reconstructed total CO_2 contents, i.e. glass plus bubble, in MIs with <10 vol% bubble fraction are between 3800 and 13700 ppm (Fig. 5). These results demonstrate the importance of CO_2 degassing into inclusion-hosted bubbles, and suggest that glass CO_2 contents measured in El Hierro MIs represent minimum melt CO_2 contents, in agreement with (Longpré et al., 2017).

5. Discussion

5.1. Crystallisation and mixing of El Hierro magmas

Melt inclusions can be trapped at any point along a crystallisation pathway. By modelling liquid lines of descent (LLDs) from primitive lavas representative of primary melt compositions, the extent of crystallisation at the time of entrapment can be determined. We used Petrolog3 (Danyushevsky and Plechov, 2011) to calculate possible LLDs for El Hierro magmas (Fig.3). Input starting compositions were 17 whole-rocks with MgO >10 wt% (Carracedo et al., 2001; Longpré, 2009; Day et al., 2010). Figure 3 shows LLDs calculated assuming an initial 1 wt% H_2O, consistent with our mean and median melt inclusion H_2O concentrations (0.9 and 0.95 wt%, respectively) and the 0.71-1.49 wt% H_2O concentrations based on clinopyroxene H_2O contents in the western Canary Islands (Weis et al., 2015). Oxygen fugacity was specified as an Fe^{3+}/Fe^{2+} ratio of 0.35 (Longpré et al., 2014, 2017). We used the mineral-melt equilibrium models of Putirka (2005) for olivine,

Danyushevsky (2001) for clinopyroxene and plagioclase, and Ariskin and Barmina (1999) for magnetite. Further details of Petrolog3 calculations are provided as supplementary material.

In all calculated LLDs, the first crystallizing phase is olivine (Fig. 3). After 7.7–19.3% olivine crystallization, the melt reaches saturation in clinopyroxene and titaniferous magnetite. This is consistent with observed phase relations in our samples: crystals of Ti-rich magnetite are absent in MgO-rich MIs hosted in Fo>82 olivines, but are common in MgO≤6 wt% inclusions. The calculated LLDs predict that plagioclase saturation is reached at melt MgO contents around 5-5.5 wt%. However, plagioclase is rarely present in our most MgO-poor tephra samples as a phenocryst phase, nor is it observed as an included crystal in any MI: it is mostly present as microlites in the groundmass. Plagioclase saturation is depressed to lower temperatures in melts with high H_2O contents, so it is possible that the 1 wt% H_2O assumed for our starting compositions underestimates the true H_2O content of some El Hierro primary melts (e.g. Sabinosa and Tamaduste) (Longpré et al., 2017). Using 0.5 to 2 wt% H_2O contents do not change the shape of LLDs and crystallising assemblage significantly, indicating this interval is the reasonable initial H_2O content for our crystallisation modelling. (Fig. S4).

Melt inclusion trace element contents are broadly consistent with crystal fractionation-dominated trends: concentrations of incompatible trace elements such as Zr increase with decreasing Mg# of the host mineral (Fig. 4B). However significant variability can be observed in the Zr content of MIs hosted crystals with similar Mg#. Large variability is observed in trace element ratios such as La/Yb, La/Y, Sm/Yb and Nb/Zr, both within individual samples and between samples from different eruptions (Fig. 4C), even though these ratios are not expected to vary significantly during crystal fractionation. Melt inclusions from Montañita Negra and Tamaduste show no significant variation in La/Yb as a function of olivine Fo content (Fig. 4C), as expected during crystal fractionation. The large varia-

tion in La/Yb (15-58) in Tanganasoga MIs is less straightforward to explain. Our data do not provide conclusive evidence that this variation is caused by mixing of magmas with differing La/Yb accompanied by crystallisation, since we do not observe decreasing variability in La/Yb with decreasing host Fo content: instead, the Tanganasoga MIs are largely restricted to host olivine compositions of $Fo_{79\pm1}$. A single crystallizing magma cannot explain the observed trace element ratio (La/Yb, La/Y, Sm/Yb and Nb/Zr) variations. We propose that the Tanganasoga MIs represent multiple magma batches that were stored separately, and were mixed prior to eruption. In this scenario the most enriched and depleted endmembers must have La/Yb>50 and La/Yb<15 respectively, and similar major element compositions, since the Tanganasoga olivines are relatively uniform in composition and show no chemical zonation. Variations in melt inclusion La/Yb could also be achieved through restricted mixing between melts already stored in a chamber and new intruding batches of melt. A third possibility is that part of the Tanganasoga crystal cargo was entrained from one or more mush zones whose crystals trapped MIs with different La/Yb to the Tanganasoga carrier melt.

Magma storage depths of 10-30 km have been calculated using clinopyroxene-liquid thermobarometry on samples from the 2011-2012 eruption and dredged rock samples along the rift axis (Stroncik et al., 2009; Longpré et al., 2014; Klügel et al., 2015). These depth estimates suggest a vertically extensive magma storage system beneath El Hierro: a suitable environment for magmas to evolve separately with little mixing. We suggest that the Tanganasoga magmatic plumbing system comprises multiple interconnected sills over a depth range of ~10-15 km, and that mixing between melts stored in these reservoirs, and possibly crystal entrainment, could reproduce the trace element characteristics observed in Tanganasoga MIs.

5.2. *Volatile budget and degassing of El Hierro magmas*

The presence of large bubbles (>10 vol.%) within our MIs suggest trapping from volatile-saturated melts. We used D-Compress (Burgisser et al., 2015) in the C-S-O-H-Fe system to calculate MI volatile saturation pressures. D-Compress requires oxygen fugacity as an input parameter, so it should be suitable for calculating volatile solubility in relatively oxidised alkaline melts. The isobars shown on Fig. 5 were calculated at 1200 °C using a melt composition representing the Tanganasoga ankaramite at clinopyroxene saturation. We assumed an fO_2 of ΔNNO=1.5 at 300 MPa and 1200 °C, based on the fO_2 estimate of Longpré et al. (2014, 2017). Isobars calculated using the most primitive and most evolved MI compositions differ by less than the 1σ analytical uncertainty on the measured MI H_2O and CO_2 contents.

Taking only glass CO_2 contents into account, the highest calculated volatile saturation pressures are between 150-355 MPa for individual samples. For MIs where both glass and bubble CO_2 contents were measured, calculated pressures using the total inclusion CO_2 reach 350-700 MPa (Fig. 5A, C). Applying the pressure-depth conversion of Longpré et al. (2014), these values corresponds to depths of 6-13 km (glass only) and 13-24 km (glass=bubble), respectively. These volatile saturation pressures should be regarded as minima, since the glass CO_2 content does not take into account any CO_2 degassed into a vapour bubble after inclusion trapping. Pressures calculated using the total CO_2 contents are consistent with both clinopyroxene-liquid barometry (400-900 MPa) and with fluid inclusion data (300-500 MPa) from previous studies (Hansteen et al., 1998; Stroncik et al., 2009; Longpré et al., 2014; Klügel et al., 2015). These pressures likely represent the main magma storage system beneath El Hierro.

D-Compress predicts sulfur solubility in the El Hierro melts to be up to 0.6 wt% at 200 MPa, and 1.1 wt% at 750 MPa, meaning MIs are unlikely to have experienced extensive S degassing. Our D-Compress calculations predict that MIs were trapped from melts domi-

nated by S^{6+} rather than S^{2-}, consistent with the high melt inclusion S contents. Very few MIs contained sulfides ($\sim 4\%$), and sulfides were not observed in the tephra groundmass. No strong correlation is present between FeO and S content in MIs, and there is no difference between the S content of sulfide-bearing and sulfide-free inclusions. We suggest that inclusion-hosted sulfides could be formed after trapping, in response to decreasing sulfur solubility during diffusive Fe loss (Danyushevsky et al., 2002), or due to a decrease in MI fO_2 as a result of lattice diffusion of Fe^{+2} via the host olivine (Gaetani et al., 2012).

The Tanganasoga melt inclusions show near-constant H_2O contents that do not decrease with decreasing sulfur (Fig. 5B). These near-uniform water contents suggest that diffusive re-equilibration has occurred between MI and the external melt, via H^+ diffusion through the host olivine. This process occurs on timescales of hours to days at magmatic temperatures (Gaetani et al., 2012). The H_2O contents of Tanganasoga MIs, and possibly those from other eruptions, likely record the water content of the pre-eruptive magma rather than their original trapped water contents (Hartley et al., 2015).

The observed H_2O-CO_2-S variations in El Hierro MIs are broadly consistent with calculated closed-system degassing pathways (Fig. 5A, C). There is a near-constant offset of ~1500 ppm S between the modelled degassing curves and our measured melt inclusion S contents (Fig. 5C): this may be an artefact of the D-Compress model, which predicts melt sulfur contents up to 2000 ppm higher than other volatile saturation models such as SolEx Witham et al. (2012). Matrix glasses contain <500 ppm S, indicating 85-90% is degassed during ascent and eruption.

Volatile-trace element ratios of an undegassed melt such as CO_2/Ba or CO_2/Nb are not expected to vary during melting or crystallisation, meaning that Ba and Nb can be used as proxies for the original melt CO_2 content (Saal et al., 2002; Rosenthal et al., 2015). Undegassed OIBs are expected to have CO_2/Nb=505±168, and CO_2/Ba=133±44 (Rosenthal et al., 2015). Our MIs have glass CO_2/Nb values <48 and CO_2/Ba<10 (Fig. 6A). Using

reconstructed total CO_2, CO_2/Ba and CO_2/Nb increases to 9-31 and 51-181, respectively. We suggest that even reconstructed MI CO_2 contents represent a partially degassed melt. Exsolution of CO_2-rich fluid likely started at pressures >1 GPa, significantly deeper than melt inclusion trapping (Longpré et al., 2017; Boudoire et al., 2018). Assuming a primary melt CO_2/Ba of 89 and using the OIB mantle CO_2 content (600 ppm) of Rosenthal et al. (2015), we calculate that our inclusions represent melts that had degassed at least 65% of their original CO_2. Using a CO_2/Nb instead of CO_2/Ba increases our estimate of pre-entrapment CO_2 degassing to >80%.

Several inclusion-hosted bubbles that occupied a large volume fraction (>10%) of the inclusion, therefore likely formed due to heterogeneous trapping of a fluid and a melt rather than by simple shrinkage (Steele-MacInnis et al., 2017), did not contain detectable CO_2. We suggest empty bubbles are formed due to MI decrepitation, whereby the fracturing of the host mineral causes loss of the vapour phase. Decrepitation is induced when internal MI and external melt pressure difference exceeds ~200 MPa (Maclennan, 2017), promoted by rapid magma ascent and low PEC. We suggest that the preservation of CO_2-rich bubbles in MIs from Tanganasoga, Sabinosa and Tamaduste could reflect relatively slow magma ascent or long residence times accompanied by cooling, which provides sufficient time for PEC to maintain the inclusion internal pressure below the decrepitation threshold. At other locations, faster magma ascent may have induced decrepitation, leading to CO_2 loss from the bubbles. Longpré et al. (2017) favoured CO_2 loss through decrepitation to explain low volatile saturation pressures (<260 MPa) for olivine-hosted MIs from the 2011-2012 eruption. We suggest that the 2011-2012 eruption and those of the Montañita Negra and Mercade cinder cones experienced similar magma ascent rates.

Melt inclusions and matrix glasses have very similar F and Cl contents (Fig. S5), suggesting that the melts experienced minimal halogen degassing. Furthermore, the MIs have F/Nd and Cl/K either above or within the expected ranges for primitive mantle-derived

melts (Fig. 6B). It has been suggested that fluorine in MIs is susceptible to diffusive re-equilibration with the surrounding melt (Koleszar et al., 2009; Le Voyer et al., 2014); however, reheating experiments do not appear to influence melt inclusion F contents (Portnyagin et al., 2008; Bucholz et al., 2013). Fluorine diffusivity in olivine has not been precisely measured, so we cannot calculate the possible effects of diffusive F exchange between our MIs and their carrier melts. However, we can rule out F enrichment through trapping of incompatible-enriched boundary layers: boundary layer effects are thought only to affect MIs smaller than 20 μm (Danyushevsky et al., 2002), and we observe no systematic change in F content as a function of inclusion size (Fig. S3). The consistency between MI and matrix glass F/Nd values, and the fact that F and Cl are positively correlated (Fig. S5), leads us to conclude that F concentrations in our MIs have not been modified by diffusion above analytical uncertainty.

5.3. Trace element characteristics of the El Hierro mantle

Canary Island magmas have been suggested to originate from a mantle source that is heterogeneous on the scale of the archipelago, with melting in asthenospheric and lithospheric mantle domains (Hoernle and Schmincke, 1993; Lundstrom et al., 2003). Stable and radiogenic isotopic data from whole-rock samples suggest the presence of lithological heterogeneities beneath La Palma and El Hierro in the form of recycled oceanic crust and lithosphere (Day et al., 2010; Day and Hilton, 2011).

While whole-rock samples represent the mixed average composition of melts supplied to a magmatic system, melt inclusions may preserve records of diverse mantle-derived melts. To explore the significance of trace element variability of our MIs, we carried out melting calculations using various mantle source compositions (Fig. 7), including the primitive mantle (PM) estimate of Hofmann (1988). We then calculated possible enriched mantle compositions by adding an eclogite-derived melt to this PM composition. Eclogite

represents a subducted oceanic crustal component in the source, and acts as a Si- and trace element-enriched metasomatising agent. Our eclogite-derived melt represents 15% melting of the median eclogite composition of Barth et al. (2001). This melt was mixed into a PM matrix in proportions of 5 and 10%. We assume that mixing occurs in a chemically closed system and that all melt reacts with peridotite to form orthopyroxene from olivine. Detailed derivations of the enriched mantle compositions are provided as supplementary material.

Our calculations suggest that the trace and rare earth element (REE) contents and ratios of El Hierro MIs are best explained by 1-8% melting of a garnet lherzolite with composition close to PM (Fig. 7). Apart from one inclusion, all our data fall within the range covered by the PM and the 5% enriched mantle melting curves. The outlier MI is extremely depleted in heavy REEs and Y, and falls between the 5 and 10% enriched garnet lherzolite melting curves. Enriched spinel lherzolite-derived melts could match the compositions of some inclusions from Montañita Negra, but do not reproduce the compositions of any other samples. Our calculated melting degrees are lower than for Hawaiian alkaline basalts (8-12%; Feigenson et al. (2003)), which could reflect lower mantle temperatures in the Canary Islands compared to Hawaii (Herzberg and Asimow, 2008). Our melting degrees are more comparable to continental alkaline basalts (e.g. McGee et al., 2013). As melting seems to be restricted to the garnet stability field, it likely occurs below the spinel-garnet transition at 2.5 GPa (80 km at 1450 °C, Klemme and O'Neill (2000). This is consistent with melting of an asthenopheric source below >90 km-thick Jurassic lithosphere (Fullea et al., 2015), and is similar to previous estimates of melting depths beneath the western Canary Islands (Day et al., 2010). It is also consistent with the ~2-6% melting of a PM-dominated source (Day et al., 2010), with possible contribution from carbonated peridotites, suggested to explain the melt volatile systematics of the 2011-2012 eruption (Longpré et al., 2017). The 1-8% variability in melting degree either reflects minor vari-

ations in temperature in the source (mantle potential temperatures for the Canary Islands are estimated around 1420-1480 °C; Herzberg and Asimow (2008)), or slight changes in mantle lithology, for example varying amounts of recycled lower lithospheric mantle (more refractory), primitive mantle, and recycled altered oceanic crust/uppermost oceanic mantle (more fusible).

5.4. Volatile characteristics of the El Hierro mantle

Determining the volatile element character of the source region of basalts is challenging. Both CO_2 and H_2O in our MIs have been modified through degassing, decrepitation and/or diffusion. However, the Ba concentrations of the most primitive MIs can be used alongside published CO_2/Ba values for the primitive mantle to estimate undegassed carbon contents for the primary magmas. We used three estimates of primitive mantle carbon content (241 ppm, Hirschmann (2016); 600 ppm, Rosenthal et al. (2015); 2803 ppm, Marty (2012)) and calculated melting curves for these compositions (Fig. 8). We then selected the MIs with the highest MgO and lowest ILE concentrations from each sampled location, and used source CO_2/Ba estimates of 40, 60, 80 and 100 (lighter to darker colour circles in Fig. 8) to estimate a range of potential original magmatic CO_2 contents. Minimum and maximum initial CO_2 contents for El Hierro magmas are estimated at 0.9% and 4.2% respectively. These values correspond to mantle CO_2 between 203 and 675 ppm, similar to estimated carbon contents for OIB mantle (Rosenthal et al., 2015) and bulk silicate Earth (Hirschmann, 2016). Using the reconstructed MI CO_2 contents together with CO_2 melting models (Fig. 8), a more conservative estimate of 120-300 ppm source CO_2 is derived, which also overlaps with the Hirschmann (2016) estimate (Fig. 8).

Our magmatic CO_2 estimates of 0.9-4.2 wt% indicate that a typical El Hierro eruption would emit 9-42 g CO_2 per kg of erupted magma. This is up to two orders of magnitude larger than the estimate for MORB magmas (0.27-3.9 g/kg, Cartigny et al. (2008)), and

also larger than the 5.7 g/kg calculated for the 2014 Holuhraun eruption (Bali et al., 2018) or the 7.5 g/kg for the 1783 Laki eruption (Hartley et al., 2014), Iceland. However, it is comparable to the estimates of 3.5±1.4 wt% CO_2 (21-49 g/kg) for Piton de la Fournaise, Réunion (Boudoire et al., 2018). These results emphasise that volatile emissions from volcanoes are not uniform globally: relatively smaller systems, such as ocean islands with enriched mantle source signatures (e.g. Canary Islands, Cape Verde, Cook Islands, St. Helena, Azores) can contribute disproportionately more to global CO_2 fluxes than their size would indicate.

If we assume that the sulfur contents of the most primitive MIs (Fig. 5) represent undegassed melts, then the primary melt is estimated to contain 3500-4500 ppm S. This melt S content can be modelled by 2-8% melting of a mantle with 265-450 ppm S, if a bulk distribution coefficient $D^S_{peridotite/melt}$ = 0.062 is used. This value is calculated assuming S has distribution coefficients similar to Dy in olivine, orthopyroxene and clinopyroxene (McKenzie and O'Nions, 1991), and is incompatible (D=0.001) in garnet. We note that mineral/melt partitioning is unlikely to dictate S behaviour during melting, which is more likely controlled by the availability of accessory sulfides and oxygen fugacity. A lower estimate of 240-340 ppm S in the source mantle can be calculated from the highest S/Dy measured in the MIs (370-530) and assuming a Dy concentration of 0.6378 ppm (Hofmann, 1988). Most estimates of primitive mantle sulfur fall between 120 and 310 ppm (Palme and O'Neill, 2003; Lyubetskaya and Korenaga, 2007), while DMM contains around 90-150 ppm S. Our calculations suggest that the El Hierro mantle source represents the S-rich end of primitive mantle estimates, or could be even more enriched.

Our melt inclusion Cl/K values of 0.04-0.10 are consistent with melts derived from a primitive mantle source, which are expected to have Cl/K=0.11±0.05 Palme and O'Neill (2003). However, our MI F/Nd values of 18-57 are higher than the 19±7 expected for primitive mantle-derived melts (Palme and O'Neill, 2003). Assuming K=258 ppm and

Nd=1.19 ppm for the primitive mantle (Hofmann, 1988), we calculate F and Cl concentrations of 20-67 ppm and 13-26 ppm, respectively, for the El Hierro mantle source.

5.4.1. Volatile recycling beneath the western Canary Islands

Our data demonstrate that El Hierro eruptions are fed by magmas that are C-, S- and F-rich in comparison with other oceanic islands like Hawaii (Moussallam et al., 2016; Anderson and Poland, 2017), and have volatile concentrations that closely resemble magmas erupting at intra-continental rift settings such as Erebus or the East African rift system (Oppenheimer et al., 2011; Moussallam et al., 2014; Hudgins et al., 2015).

Our calculated F content for the El Hierro mantle source, 20-63 ppm, is elevated compared to primitive mantle. This F enrichment is accompanied by relatively low source Cl of 13-26 ppm, which rules out crustal or seawater assimilation. We suggest that the F enrichment is best explained by the presence of a recycled crustal component in the source. This is in accordance with previous results from HIMU-type OIBs from the Pacific Ocean (Cabral et al., 2014) and from the Azores (Rose-Koga et al., 2017), where elevated F/Nd in MIs was interpreted as a signature originating from recycled material in the mantle source. Subducting slabs tend to retain most of their F during dehydration, while Cl is fluid-mobile and is typically lost to escaping fluids (Kendrick et al., 2014). Recycled lithospheric components in the mantle should therefore have high F/Cl, which is then reflected in melts produced from this lithology. The sulfur concentration in the mantle source might be less important than fO_2 in controlling melt sulfur contents. El Hierro magmas have been suggested to be more oxidised than typical OIB mantle (Longpré et al., 2014, 2017), which could be a key factor in controlling the S content of the primitive melts.

Our upper estimate of 675 ppm CO_2 in the El Hierro mantle falls within the 600±200 ppm estimated for an OIB mantle source (Rosenthal et al., 2015). However, our estimate of mantle carbon is based on CO_2/Ba ratios of 40-100 in the source, lower than the CO_2/Ba

of 133±44 suggested by Rosenthal et al. (2015) for OIB mantle. It is therefore possible that the El Hierro mantle could be significantly enriched in carbon. Excess carbon could originate from recycled subducted components, which would be consistent with Os and O-isotopic data indicating the presence of altered basalts and gabbros in the source region beneath the western Canary Islands (Day et al., 2009). Carbon could be present in the source mantle as recycled carbonates like magnesite or Ca-rich dolomites, which have been suggested to be stable during slab subduction (Dasgupta and Hirschmann, 2010; Dorfman et al., 2018). Recycled carbonates are thought to melt around ~300 km, forming carbon-rich fluids which induce silicate melting in recycled oceanic crustal material. The silicate and carbonatite melts produced then enrich the surrounding mantle in ILEs and volatiles, ultimately forming a heterogeneous, volatile- and carbon-rich mantle source beneath El Hierro. These results strongly strengthen previous observations at other OIBs (Cabral et al., 2014), that the character of the mantle source plays a crucial role in influencing volcanic volatile fluxes from OIBs: similar levels of CO_2 and S enrichment are expected at other OIBs with enriched trace element and isotopic composition both in the case of neighbouring islands chains (Cape Verde, Azores, St. Helena) and globally (e.g. Cook Islands).

6. Conclusions

Olivine- and clinopyroxene-hosted melt inclusions from young El Hierro basanites show considerable variability in trace element contents and ratios, and some of the highest CO_2, S and F contents measured in MIs from oceanic islands to date. Major element systematics show that MIs are trapped at all stages along the crystallization path. Some primitive eruptions carry Fo-rich olivines hosting high-MgO MIs, while others produced more evolved clinopyroxene- and oxide-saturated magmas. Melt inclusion incompatible trace element ratios like La/Yb are significantly variable even within single eruptions, in-

dicating that MIs were trapped from several magma batches that evolved separately from one another (Fig. 9). Trace element variability likely formed by mantle processes, e.g. variable melting degree of the mantle source. Since the variability in trace element ratios occurs in MIs with similar major element compositions and does not decrease with decreasing host olivine Fo content or clinopyroxene Mg#, they must represent melt batches formed either by different melting degrees, or by melting a heterogeneous mantle source. We propose a magmatic system comprising multiple interconnected sills (Stroncik et al., 2009; Klügel et al., 2015) whereby, during eruptions, multiple sills are tapped and mixed to produce a magma with a crystal cargo hosting MIs with highly variable trace element characteristics.

In this extensive plumbing system, various processes influence volatile systematics of the melt, both within the whole system and inside the melt inclusions. Up to 85% of melt inclusion CO_2 may be sequestered into inclusion-hosted bubbles formed by post-entrapment degassing during storage. Reconstructed total MI CO_2 concentrations (glass plus bubble) are >1.0 wt%, corresponding to volatile saturation pressures up to 700 MPa. Melt inclusion CO_2/Ba values of <31 are significantly lower than expected for undegassed, mantle-derived magmas, indicating that El Hierro magmas exsolved considerable CO_2 prior to inclusion trapping. Original melt CO_2 contents are likely between 0.9 and 4.2 wt%, with the precise value dependent on the mantle carbon content and melting degree. El Hierro MIs have high F concentrations and F/Nd values, which we suggest reflects a mantle source enriched in F relative to primitive mantle, most probably a recycled oceanic lithospheric component. Calculated sulfur and carbon contents for the mantle source are at the upper limit of published estimates for primitive mantle. Recycled C and S in the Canary Island mantle would provide a possible explanation for the formation of a trace element-enriched, heterogeneous mantle source beneath El Hierro, whereby volatile-induced melting of recycled crustal eclogites or pyroxenites metasomatises and enriches

the asthenospheric mantle. Original melt CO_2 estimates presented here indicate eruptions of El Hierro, and more widely small oceanic islands where the presence of recycled crustal material in the mantle source is common, can contribute disproportionally more volatiles than their Icelandic or MORB counterparts. Our results demonstrate the usefulness of melt inclusions as a tool for tracing volatile recycling into the mantle, the importance of alkaline basaltic volcanism to fluxes of deep volatiles into the environment, and the influence of subduction-related volatile recycling to the mantle on global oceanic island volatile emissions.

Acknowledgements

This work was supported by NERC studentship NE/L002469/1 to ZT, and NERC grant IMF600/1016. We thank Alex Nichols and two anonymous reviewers for their constructive and helpful reviews, which greatly improved the quality of this manuscript. We thank Cees-Jan de Hoog at the Edinburgh Ion Microprobe Facility for his assistance during the ion probe analyses; Jonathan Fellowes for the assistance with the electron miroprobe in Manchester; Iris Buisman for assistance with electron microprobe work in Cambridge; and Heath Bagshaw and Mehul Chavda for assistance with Raman spectrometry. MH and ME acknowledge Conny Spelbrink and Paul Hartley for assistance with various aspects of the field work and sample collection.

Figures and figure captions

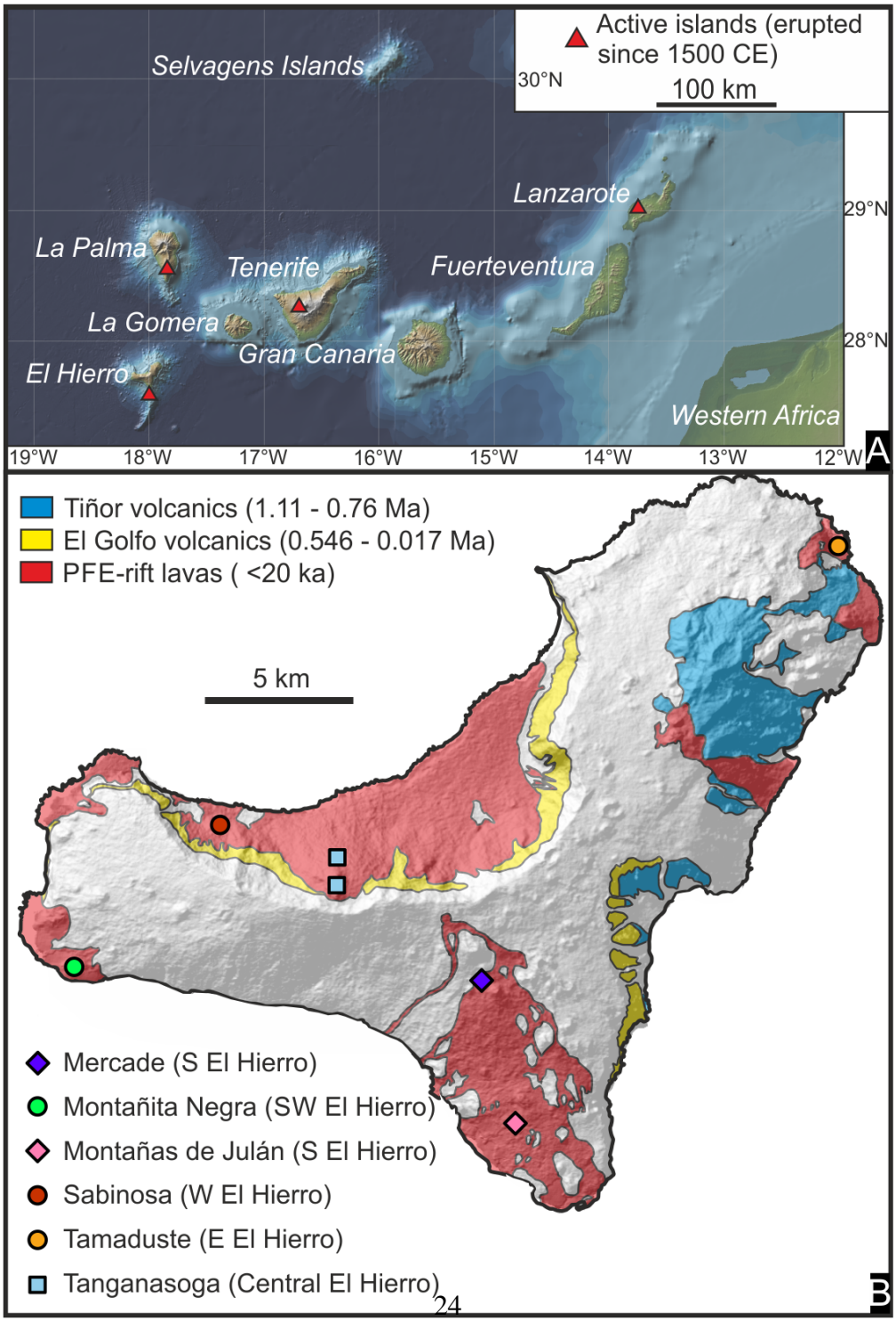

Figure 1. (A) Topographic map of the Canary Islands constructed using GeoMapApp (`https://www.geomapapp.org/`), showing the locations of post-1500 CE eruptions: 13 eruptions occurred in the last 500 years, the last being the submarine eruption 2 km south off the coast of El Hierro in 2011-2012. As seen in (A), the southern arm of the El Hierro rift system extends several kilometres into the Atlantic Ocean. (B) Simplified geological map of El Hierro, modified after Carracedo et al. (2001) with digital elevation model from GeoMapApp. The map shows the erupted products from the three main volcanic edifices (Tiñor, El Golfo and the rift volcanics) that have built the island, and the sample locations for this study.

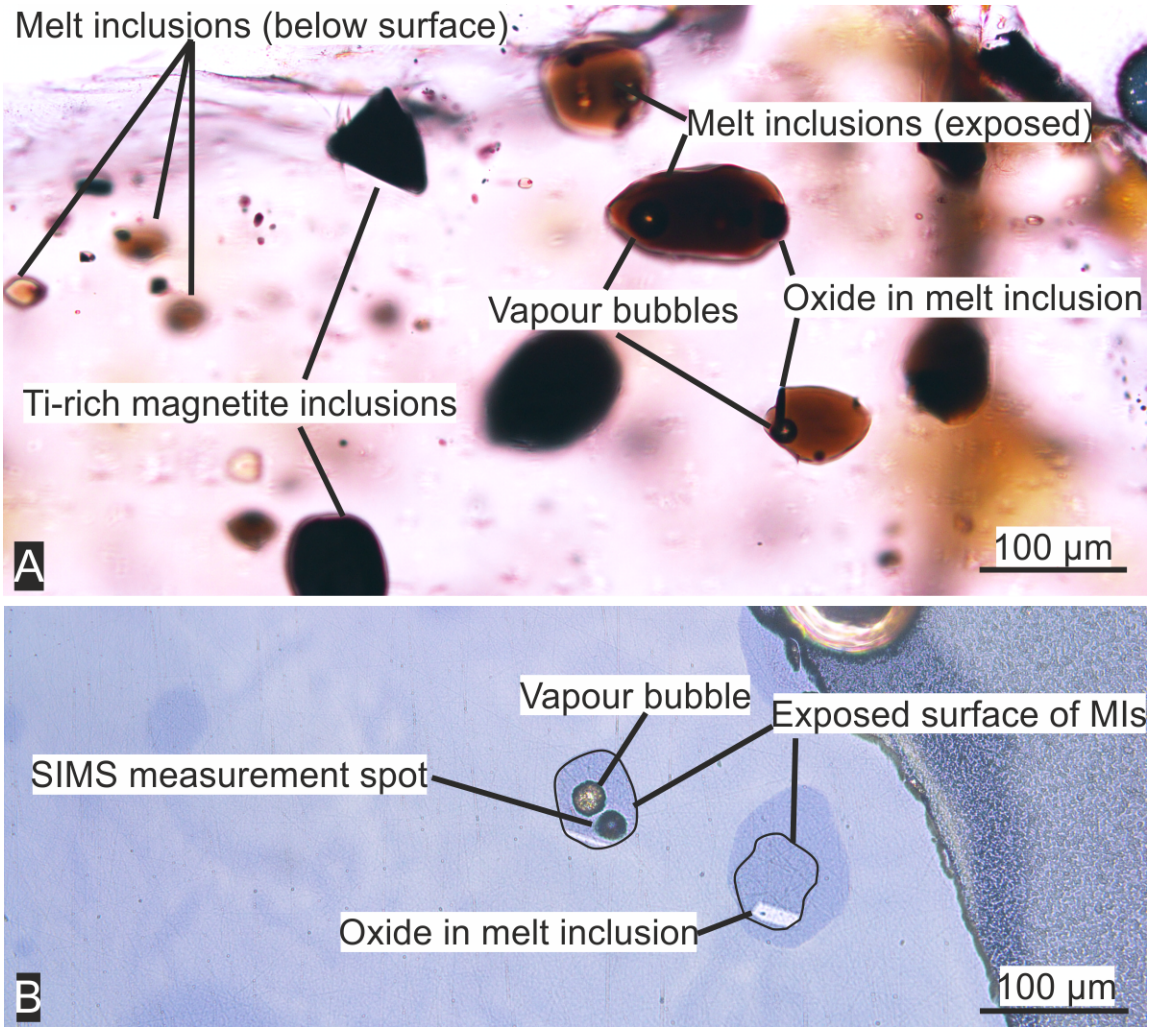

Figure 2. (A) Transmitted and (B) reflected light images of olivine crystals from El Hierro, each containing several melt inclusions. The inclusions are dominantly glassy, and may contain bubbles and crystals of Ti-rich magnetite and, rarely, clinopyroxene. The inclusion-hosted oxides are interpreted as being captured during multi-phase entrapment of melt and solid, since the volumetric proportion of oxide in the inclusions (typically >10 vol.%) is much larger than expected for post-entrapment formation of daughter crystals. Small, globular sulfides, such as in the lower exposed inclusion in (A), probably precipi-

551 tated after inclusion trapping in response to the decrease in S solubility that accompanies
552 diffusive Fe loss from the trapped melt (Danyushevsky et al., 2002).

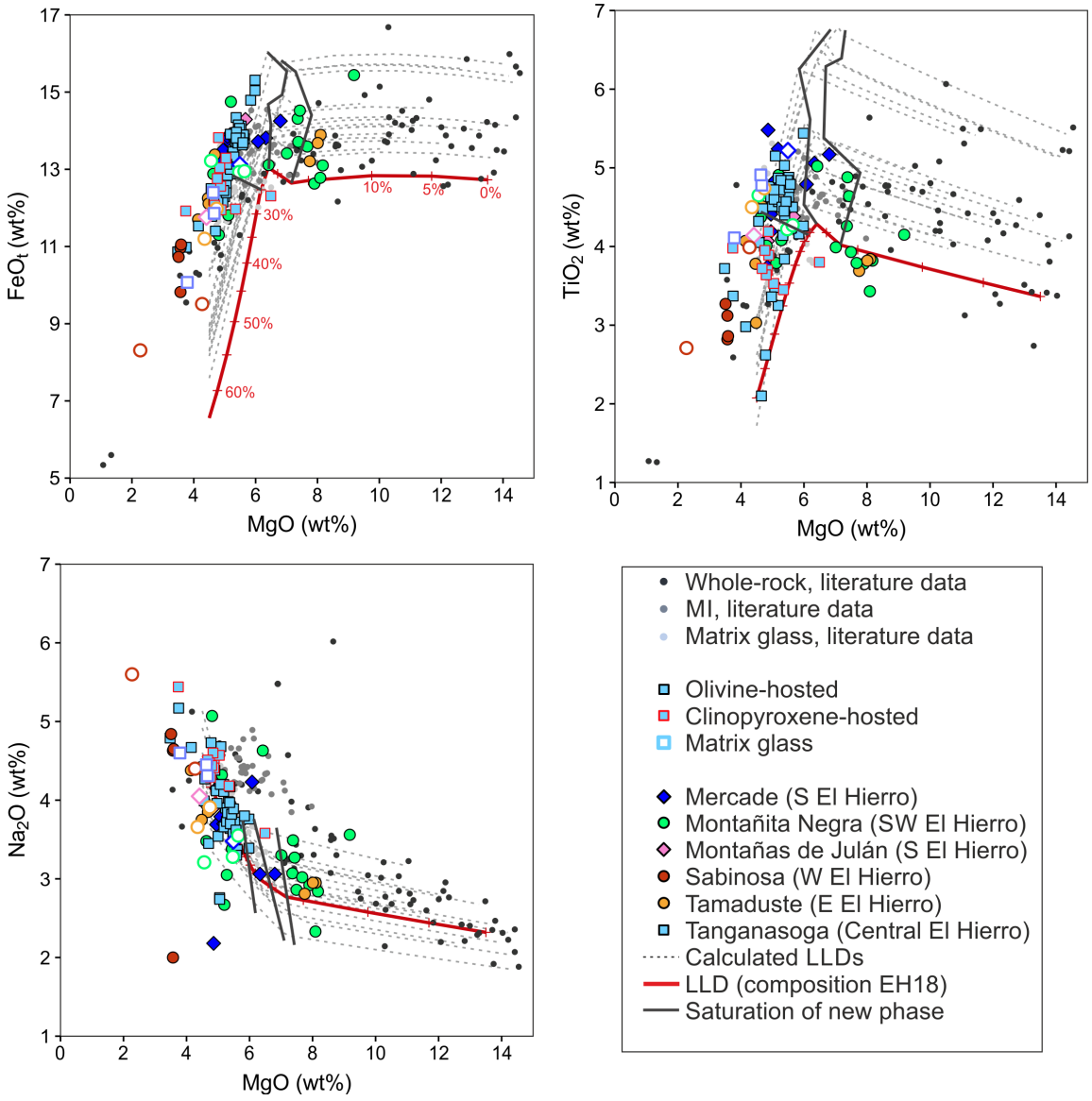

Figure 3. Major element contents of melt inclusions (filled symbols) and matrix glasses (open symbols), together with literature data from El Hierro (gray and black circles; Carracedo et al. (2001); Abratis et al. (2002); Stroncik et al. (2009); Longpré (2009); Day et al. (2010); Klügel et al. (2011); Martí et al. (2013a); Longpré et al. (2017)). Black dotted lines are liquid lines of descent (LLDs) calculated from primitive lava compositions

from El Hierro using Petrolog3 (Danyushevsky and Plechov, 2011). The red dashed line is a LLD calculated from sample EH18 Longpré (2009), an olivine-phyric (FO_90) alkaline basalt thought to represent a composition close to the primary melt; this sample is not thought to be affected by crystal accumulation. LLDs are calculated assuming 1 wt% initial H_2O and a Fe^{3+}/Fe^{2+} ratio of 0.35. Red crosses along this LLD represent 5% steps in crystallisation. Total crystallisation amount varies considerably between LLDs from 37% to 63%. Thin solid lines indicate the predicted positions of clinopyroxene, magnetite and plagioclase saturation on the liquidus, in order of decreasing MgO content. Symbol size is larger than the 1σ standard deviation.

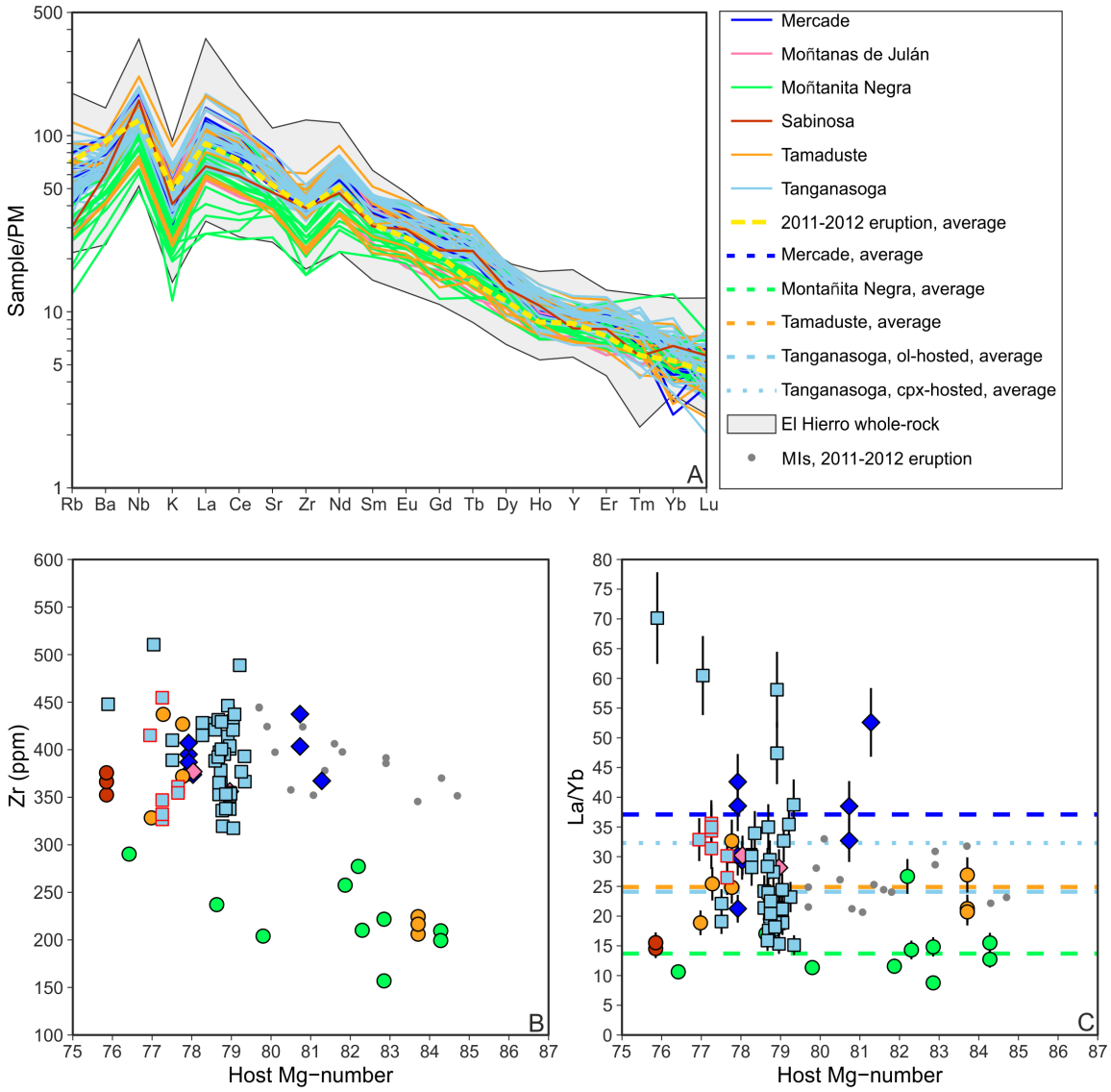

Figure 4. (A) Multi-element diagram for El Hierro matrix glasses and melt inclusions. Concentrations are normalised to primitive mantle (Hofmann, 1988). Samples fall within the range of previously measured whole-rock analyses from El Hierro (the grey shaded area includes alkali basalts and trachytes, Carracedo et al. (2001); Abratis et al. (2002); Day et al. (2010); Klügel et al. (2011); Martí et al. (2013a)) and show similar patterns

to whole-rock samples and MIs from the 2011-2012 eruption. (B) Melt inclusion Zr and (C) La/Yb vs. Mg# of the host mineral (olivine Fo mol% or clinopyroxene Mg#). Error bars are 1σ and mostly smaller than the symbol size. The dashed coloured lines show the average La/Yb for MIs from single locations. Grey circles show MIs from the 2011-2012 eruption (Longpré et al., 2017). The broad overall increase in Zr with decreasing host Mg# is consistent with crystal fractionation, but the variation in Zr and La/Yb at constant host Mg# cannot be explained by crystallisation of a single initial melt composition. This may instead indicate that the magmatic systems beneath El Hierro is fed by variably enriched primary melts.

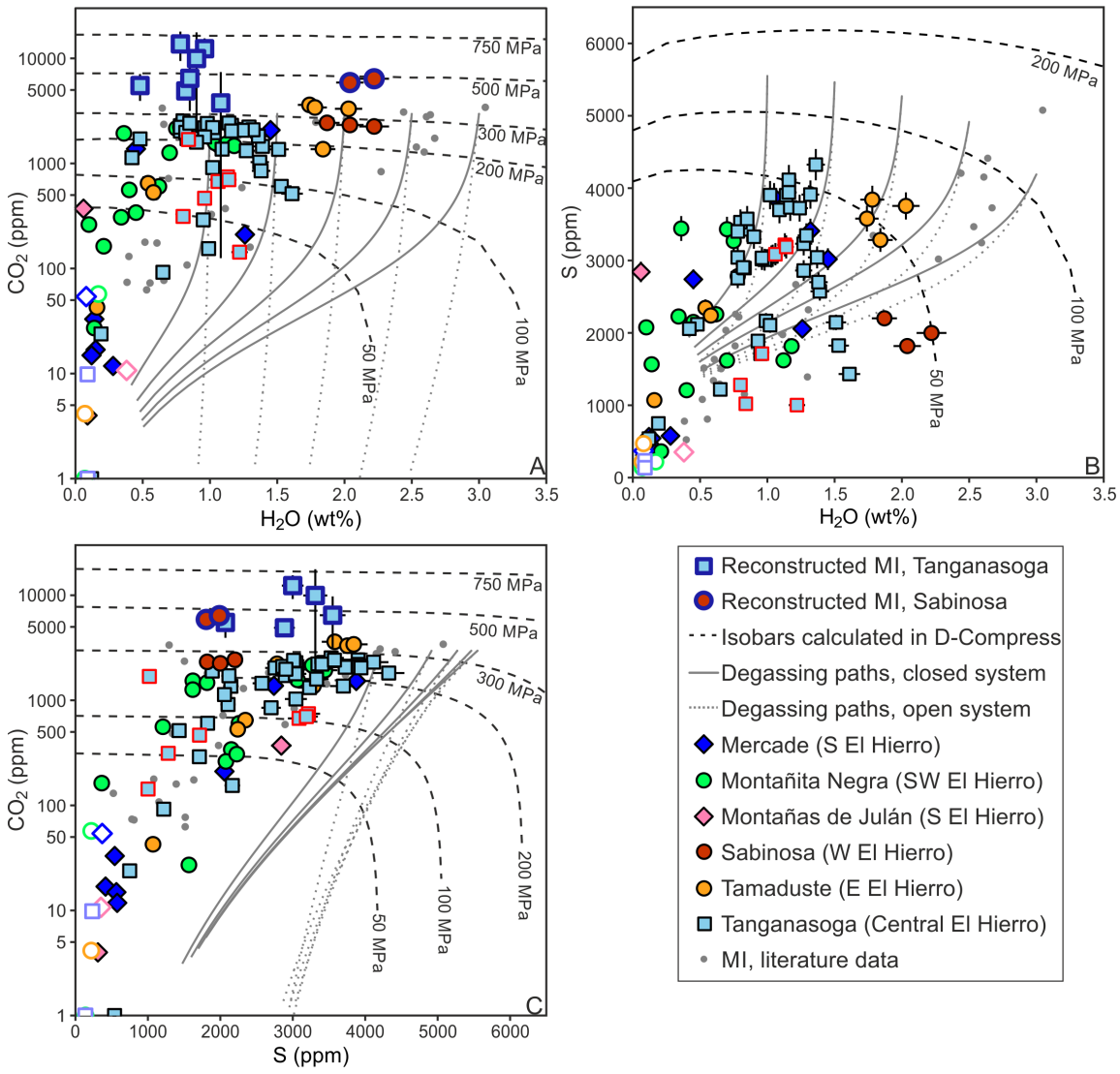

Figure 5. H_2O, CO_2 and S concentrations in the studied melt inclusions on CO_2 vs. H_2O (A), S vs. H_2O (B) and CO_2 vs. S (C). Literature data are MIs from the 2011-2012 eruption by Longpré et al. (2017). Dashed lines show isobars calculated for the H-C-O-S-Fe system using D-Compress (Burgisser et al., 2015). Isobars were calculated using a magma composition close to clinopyroxene saturation of the Tanganasoga ankaramite (43.5 % SiO_2, 4.4 TiO_2, 12.7 % Al_2O_3, 13.1 % FeO, 8.8 % MgO, 12.8 % CaO, 2.96

% Na_2O, 0.8 % K_2O), at a temperature of 1200 °C. fO_2 of ΔNNO=1.5 was used in the calculations. Degassing paths were calculated using D-Compress with the same input melt composition and temperature, a starting CO_2 of 3500 ppm, and water contents between 1 and 3 wt%. Black- and red-outlined symbols show volatile concentrations measured in the glass phase. Larger symbols with blue outlines show reconstructed total CO_2 contents, i.e. glass plus bubble. Error bars for reconstructed MI CO_2 contents are 1σ standard errors derived from the Raman peak fitting process. 1σ error bars for glass are mostly smaller than the symbol size. Volatile contents in our melt inclusions are similar to those of MIs from the 2011-2012 eruption (grey circles). Maximum volatile saturation pressures derived from glass CO_2 contents are 250-350 MPa. Using total inclusion CO_2 (glass plus bubble), maximum saturation pressures exceed 700 MPa. Isobars plotted in H_2O-S space (Fig. 5B) are much less pressure-sensitive, hence there are large uncertainties on their position.

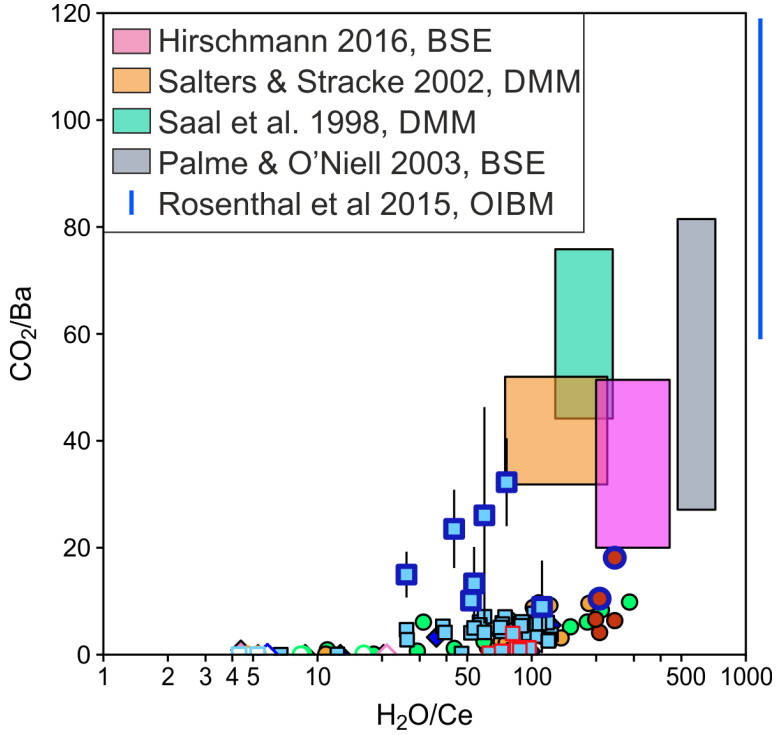
Hirschmann 2016, BSE
Salters & Stracke 2002, DMM
Saal et al. 1998, DMM
Palme & O'Niell 2003, BSE
Rosenthal et al 2015, OIBM
CO2/Ba
H2O/Ce
120
100
80
60
40
20
0
1
2
3
4
5
10
50
100
500
1000

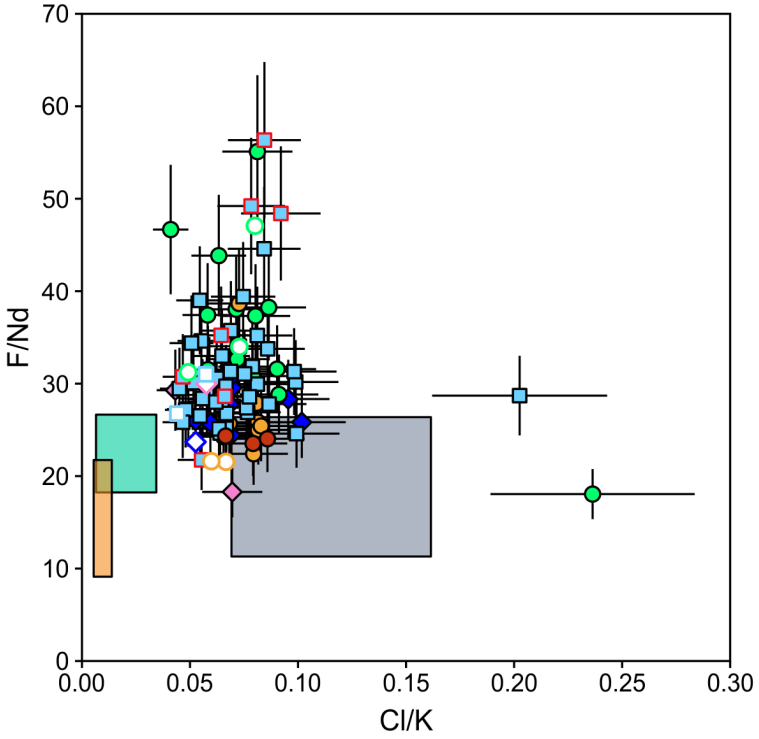
F/Nd
Cl/K
70
60
50
40
30
20
10
0
0.00
0.05
0.10
0.15
0.20
0.25
0.30

Figure 6. Volatile/trace element ratios of melt inclusions: (A) CO_2/Ba vs. H_2O/Ce (note the log10 x-axis), and (B) F/Nd vs. Cl/K. Symbols are the same as in Fig. 5. Literature estimates of volatile concentrations in primitive mantle (PM) and depleted MORB mantle (DMM) are taken from Saal et al. (2002), Palme and O'Neill (2003), Salters and Stracke (2004), Rosenthal et al. (2015) and Hirschmann (2016), while trace element concentrations are from Palme and O'Neill (2003) and Salters and Stracke (2004). Rosenthal et al. (2015) did not estimate mantle water concentrations; hence we show their CO_2/Ba range as bar outside of the x-axis instead of a field in (A). Error bars are 1 σ. All the El Hierro melt inclusions have lower CO_2/Ba than would be predicted for melts derived from a PM source. Melt inclusions have Cl/K just below the expected range for PM, but have elevated F/Nd compared to both DMM and PM. This could indicate the presence of a high-F/Cl component in the mantle source.

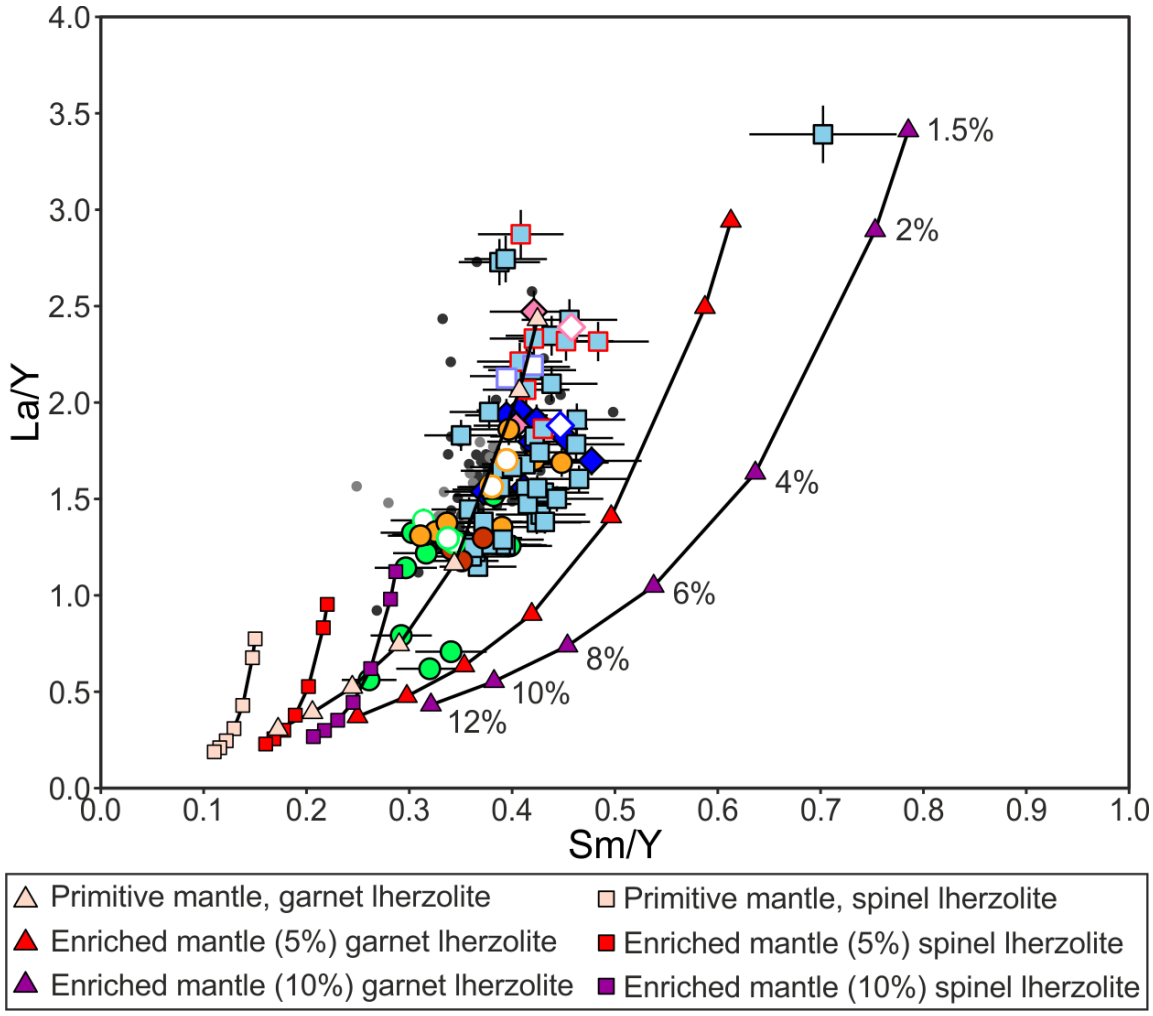

Figure 7. Mantle melting models compared with our MI dataset and whole-rock samples and melt inclusions from the 2011-2012 eruption, shown on a La/Y vs. Sm/Y diagram. Melt inclusions and literature data are shown using the same symbols as Fig 3. The primitive mantle (PM) composition is from Hofmann (1988). Enriched mantle compositions were calculated by adding 5 and 10% eclogite-derived melt to PM. Symbols on the model curves indicate the partial melt fraction (same fractions for every curve). Most El Hierro whole-rock and melt inclusion compositions fall along the garnet-bearing primitive

mantle source curve. This indicates melting depth is restricted below 80 km, i.e. below the garnet-spinel transition, which is in accordance with the presence of a >90 km-thick Jurassic lithosphere beneath the island (Fullea et al., 2015).

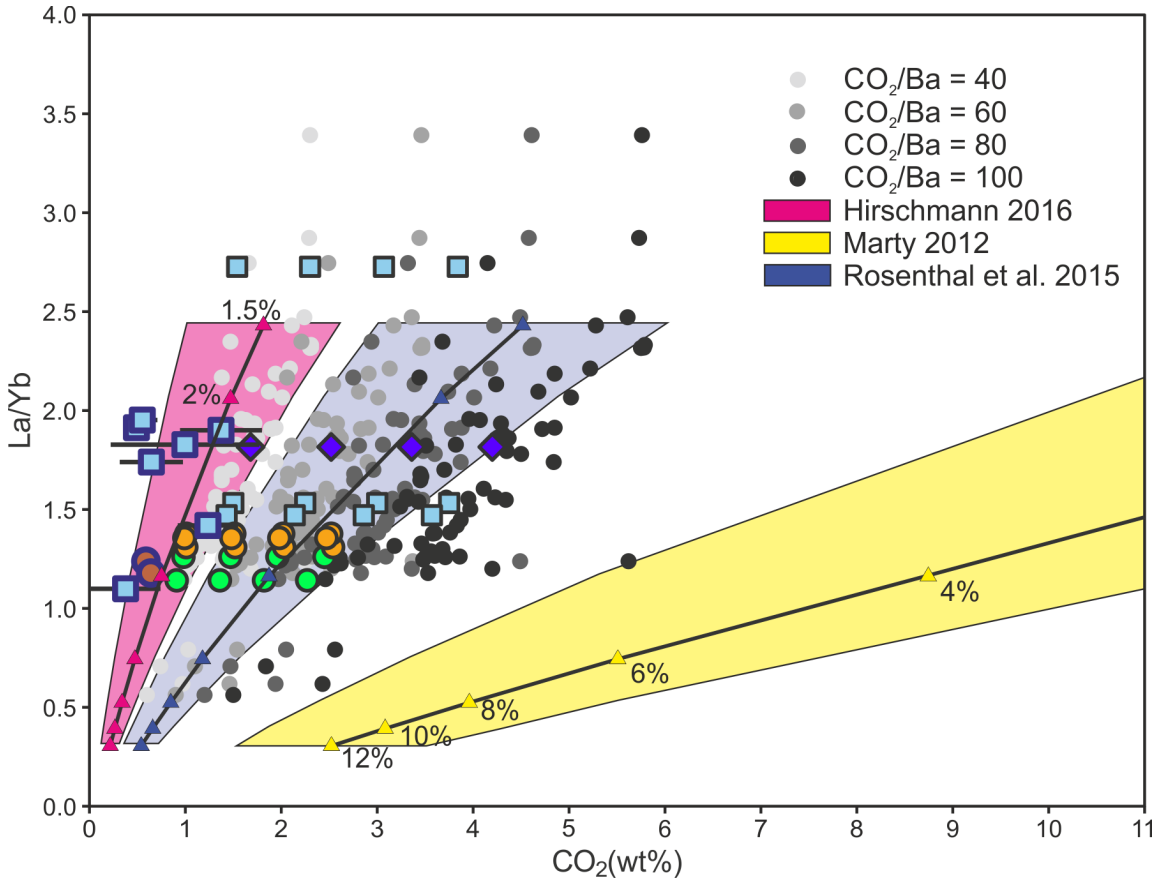

Figure 8. Estimates of original melt inclusion CO_2 contents, calculated using measured Ba concentrations and assuming a range of CO_2/Ba values (40, 60, 80 and 100) for primary mantle-derived melts, plotted against measured La/Y values. Assuming a primitive mantle Ba content of 6.75 ppm, these CO_2/Ba ratios correspond to source CO_2 contents of 270, 405, 540 and 675 ppm respectively. The melt inclusion dataset is plotted in grey, where darker shade means a higher source CO_2/Ba ratio was used to calculate the undegassed melt CO_2 content. Large, coloured symbols with black outlines (symbols as in Fig. 3) show calculated CO_2 contents for the least-evolved melt inclusions from each sample location, identified by their high MgO, low ILE contents and high host olivine Fo mol%. Higher CO_2 at identical La/Y means higher input CO_2/Ba values for these points.

Large symbols with blue outlines show measured CO_2 and La/Y for melt inclusions with reconstructed (glass plus bubble) total CO_2 contents. Black curves show primary melt CO_2 concentrations produced by melting a primitive mantle source, calculated using different published mantle carbon concentrations (Marty, 2012; Rosenthal et al., 2015; Hirschmann, 2016); labelled triangle symbols show the partial melt fraction. The shaded coloured fields for each melting model represent the uncertainty in the starting mantle carbon content.

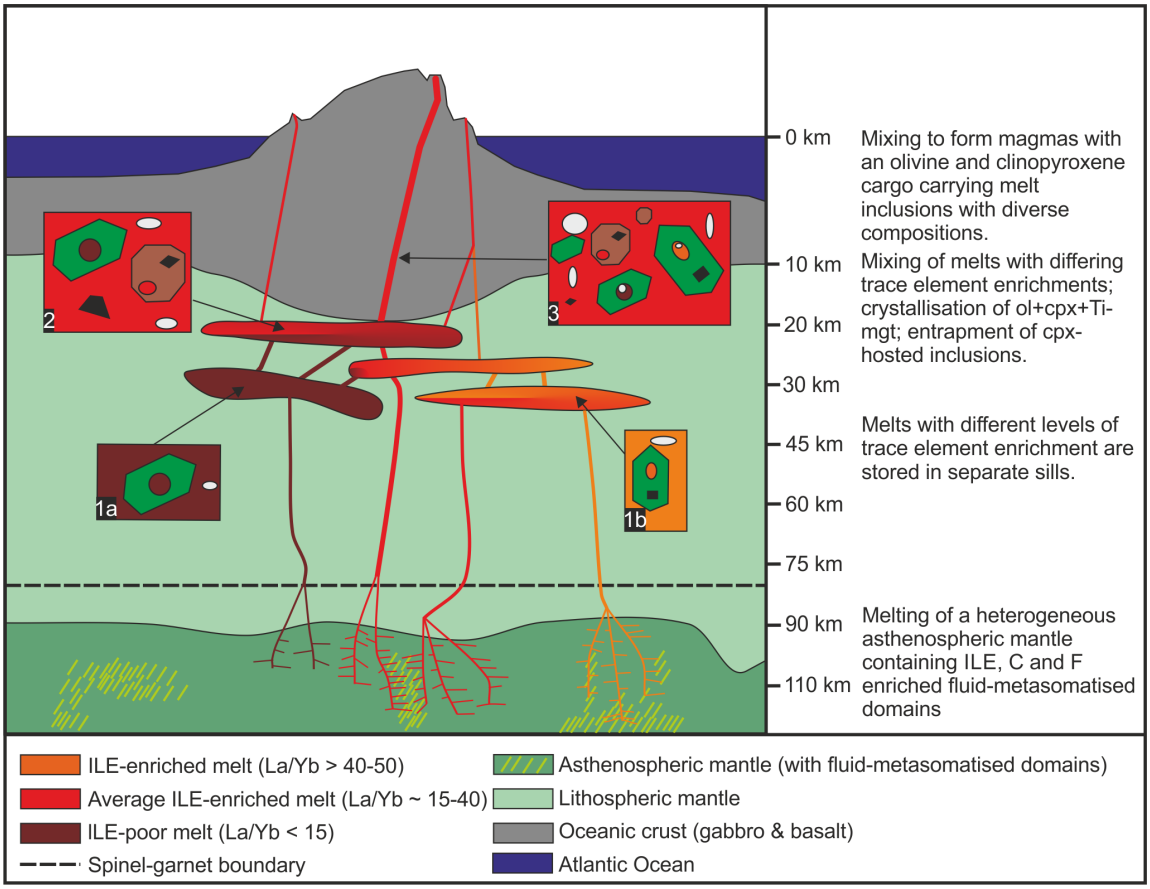

Figure 9. Schematic cartoon summarising the melt generation and evolution of El Hierro basanites. Primary melts form in the asthenospheric mantle, sampling a heterogeneous source containing a recycled oceanic lithospheric component that is enriched in incompatible lithophile elements (ILE), F, and possibly C and S. These melts ascend through the lithospheric mantle and start exsolving CO_2 at pressures >1 GPa. Partially degassed magmas are then stored within a multi-level storage system of interconnected sills. The sills can store magmas that are variably enriched in ILEs and volatiles, represented by boxes 1a and 1b (orange to dark red colours represent enrichment). Melts evolve separately within their storage reservoirs, trapping melt inclusions with differing La/Y. As the

liquids evolve they become saturated in Ti-rich magnetite and clinopyroxene (box 2) and continue to degas CO_2 together with H_2O and S. Eruptions are eventually fed by melts pooled from multiple sills, which carry a crystal cargo that hosts melt inclusions trapped from variably degassed melts and with highly variable ILE ratios (box 3).

References

Abratis, M., Schmincke, H.U., Hansteen, T., 2002. Composition and evolution of submarine volcanic rocks from the central and western Canary Islands. International Journal of Earth Sciences 91, 562–582. doi:10.1007/s00531-002-0286-7.

Anderson, K.R., Poland, M.P., 2017. Abundant carbon in the mantle beneath Hawai'i. Nature Geoscience 10, 704. doi:10.1038/ngeo3007.

Ariskin, A.A., Barmina, G.S., 1999. An empirical model for the calculation of spinel-melt equilibria in mafic igneous systems at atmospheric pressure: 2. Fe-Ti oxides. Contributions to Mineralogy and Petrology 134, 251–263. doi:10.1007/s004100050482.

Bali, E., Hartley, M., Halldórsson, S., Gudfinnsson, G., Jakobsson, S., 2018. Melt inclusion constraints on volatile systematics and degassing history of the 2014–2015 Holuhraun eruption, Iceland. Contributions to Mineralogy and Petrology 173. doi:10.1007/s00410-017-1434-1.

Balogh, K., Ahijado, A., Casillas, R., Fernández, C., 1999. Contributions to the chronology of the Basal Complex of Fuerteventura, Canary Islands. Journal of Volcanology and Geothermal Research 90, 81–101. doi:10.1016/S0377-0273(99)00008-6.

Barth, M.G., Rudnick, R.L., Horn, I., McDonough, W.F., Spicuzza, M.J., Valley, J.W., Haggerty, S.E., 2001. Geochemistry of xenolithic eclogites from West Africa, Part I: a link between low MgO eclogites and Archean crust formation. Geochimica et Cosmochimica Acta 65, 1499–1527. doi:10.1016/S0016-7037(00)00626-8.

Boudoire, G., Rizzo, A.L., Di Muro, A., Grassa, F., Liuzzo, M., 2018. Extensive CO_2 degassing in the upper mantle beneath oceanic basaltic volcanoes: First insights from

673 Piton de la Fournaise volcano (La Réunion Island). Geochimica et Cosmochimica Acta
674 235, 376–401. doi:10.1016/j.gca.2018.06.004.

675 Bucholz, C.E., Gaetani, G.A., Behn, M.D., Shimizu, N., 2013. Post-entrapment modi-
676 fication of volatiles and oxygen fugacity in olivine-hosted melt inclusions. Earth and
677 Planetary Science Letters 374, 145–155. doi:10.1016/j.epsl.2013.05.033.

678 Burgisser, A., Alletti, M., Scaillet, B., 2015. Simulating the behavior of volatiles belonging
679 to the C–O–H–S system in silicate melts under magmatic conditions with the software
680 D-Compress. Computers & Geosciences 79, 1–14. doi:10.1016/j.cageo.2015.03.
681 002.

682 Burton, M.R., Sawyer, G.M., Granieri, D., 2013. Deep carbon emissions from volcanoes.
683 Reviews in Mineralogy and Geochemistry 75, 323–354. doi:10.2138/rmg.2013.75.
684 11.

685 Cabral, R.A., Jackson, M.G., Koga, K.T., Rose-Koga, E.F., Hauri, E.H., Whitehouse, M.J.,
686 Price, A.A., Day, J.M., Shimizu, N., Kelley, K.A., 2014. Volatile cycling of H_2O, CO_2,
687 F, and Cl in the HIMU mantle: A new window provided by melt inclusions from oceanic
688 hot spot lavas at Mangaia, Cook Islands. Geochemistry, Geophysics, Geosystems 15,
689 4445–4467. doi:10.1002/2014GC005473.

690 Carracedo, J.C., Badiola, E.R., Guillou, H., de la Nuez, J., Torrado, F.P., 2001. Geology
691 and volcanology of La Palma and El Hierro, Western Canaries. Estudios Geológicos
692 57, 175–273. doi:hdl.handle.net/10261/2343.

693 Cartigny, P., Pineau, F., Aubaud, C., Javoy, M., 2008. Towards a consistent mantle carbon
694 flux estimate: Insights from volatile systematics (H_2O/Ce, δD, CO_2/Nb) in the North

695 Atlantic mantle (14 N and 34 N). Earth and Planetary Science Letters 265, 672–685.
696 doi:10.1016/j.epsl.2007.11.011.

697 Coello, J., Cantagrel, J.M., Hernán, F., Fúster, J.M., Ibarrola, E., Ancochea, E., Casquet,
698 C., Jamond, C., Díaz de Téran, J.R., Cendrero, A., 1992. Evolution of the eastern
699 volcanic ridge of the Canary Islands based on new K-Ar data. Journal of Volcanology
700 and Geothermal Research 53, 251–274. doi:10.1016/0377-0273(92)90085-R.

701 Danyushevsky, L.V., 2001. The effect of small amounts of H_2O on crystallisation of mid-
702 ocean ridge and backarc basin magmas. Journal of Volcanology and Geothermal Re-
703 search 110, 265–280. doi:10.1016/S0377-0273(01)00213-X.

704 Danyushevsky, L.V., Della-Pasqua, F.N., Sokolov, S., 2000. Re-equilibration of melt in-
705 clusions trapped by magnesian olivine phenocrysts from subduction-related magmas:
706 petrological implications. Contributions to Mineralogy and Petrology 138, 68–83.

707 Danyushevsky, L.V., McNeill, A.W., Sobolev, A.V., 2002. Experimental and petrological
708 studies of melt inclusions in phenocrysts from mantle-derived magmas: an overview
709 of techniques, advantages and complications. Chemical Geology 183, 5–24. doi:10.
710 1016/S0009-2541(01)00369-2.

711 Danyushevsky, L.V., Plechov, P., 2011. Petrolog3: Integrated software for modeling crys-
712 tallization processes. Geochemistry Geophysics Geosystems 12, 1–32. doi:10.1029/
713 2011GC003516.

714 Dasgupta, R., Hirschmann, M.M., 2010. The deep carbon cycle and melting in Earth's
715 interior. Earth and Planetary Science Letters 298, 1–13. doi:10.1016/j.epsl.2010.
716 06.039.

717 Dasgupta, R., Hirschmann, M.M., Smith, N.D., 2007. Partial melting experiments of peri-
718 dotite + CO_2 at 3 GPa and genesis of alkalic ocean island basalts. Journal of Petrology
719 48, 2093–2124. doi:10.1093/petrology/egm053.

720 Day, J.M.D., Hilton, D.R., 2011. Origin of $^3He/^4He$ ratios in HIMU-type basalts con-
721 strained from Canary Island lavas. Earth and Planetary Science Letters 305, 226–234.
722 doi:10.1016/j.epsl.2011.03.006.

723 Day, J.M.D., Pearson, D.G., Macpherson, C.G., Lowry, D., Carracedo, J.C., 2009.
724 Pyroxenite-rich mantle formed by recycled oceanic lithosphere: Oxygen-osmium iso-
725 tope evidence from Canary Island lavas. Geology 37, 555–558. doi:/10.1130/
726 G25613A.1.

727 Day, J.M.D., Pearson, D.G., Macpherson, C.G., Lowry, D., Carracedo, J.C., 2010. Evi-
728 dence for distinct proportions of subducted oceanic crust and lithosphere in HIMU-type
729 mantle beneath El Hierro and La Palma, Canary Islands. Geochimica et Cosmochimica
730 Acta 74, 6565–6589. doi:10.1016/j.gca.2010.08.021.

731 Dixon, J.E., 1997. Degassing of alkalic basalts. American Mineralogist 82, 368–378.

732 Dixon, J.E., Clague, D.A., Wallace, P., Poreda, R., 1997. Volatiles in alkalic basalts form
733 the North Arch Volcanic Field, Hawaii: extensive degassing of deep submarine-erupted
734 alkalic series lavas. Journal of Petrology 38, 911–939. doi:10.1093/petroj/38.7.
735 911.

736 Dorfman, S.M., Badro, J., Nabiei, F., Prakapenka, V.B., Cantoni, M., Gillet, P., 2018.
737 Carbonate stability in the reduced lower mantle. Earth and Planetary Science Letters
738 489, 84–91. doi:10.1016/j.epsl.2018.02.035.

739 Edmonds, M., Sides, I.R., Swanson, D.A., Werner, C., Martin, R.S., Mather, T.A., Herd,
740 R.A., Jones, R.L., Mead, M.I., Sawyer, G., Roberts, T.J., Sutton, A.J., Elias, T., 2013.
741 Magma storage, transport and degassing during the 2008-10 summit eruption at Kilauea
742 Volcano, Hawaii. Geochimica et Cosmochimica Acta 123, 284–301. doi:10.1016/j.
743 gca.2013.05.038.

744 Feigenson, M.D., Bolge Louise, L., Carr Michael, J., Herzberg Claude, T., 2003. REE
745 inverse modeling of HSDP2 basalts: Evidence for multiple sources in the Hawaiian
746 plume. Geochemistry, Geophysics, Geosystems 4. doi:10.1029/2001GC000271.

747 French, S.W., Romanowicz, B., 2015. Broad plumes rooted at the base of the Earth's
748 mantle beneath major hotspots. Nature 525, 95–99. doi:10.1038/nature14876.

749 Fullea, J., Camacho, A.G., Negredo, A.M., Fernández, J., 2015. The Canary Is-
750 lands hot spot: New insights from 3D coupled geophysical–petrological modelling
751 of the lithosphere and uppermost mantle. Earth and Planetary Science Letters
752 409, 71–88. URL: http://www.sciencedirect.com/science/article/pii/
753 S0012821X14006657, doi:https://doi.org/10.1016/j.epsl.2014.10.038.

754 Gaetani, G.A., Grove, T.L., Bryan, W.B., 1993. The influence of water on the petrogenesis
755 of subduction-related igneous rocks. Nature 365, 332. doi:10.1038/365332a0.

756 Gaetani, G.A., O'Leary, J.A., Shimizu, N., Bucholz, C.E., Newville, M., 2012. Rapid
757 reequilibration of H_2O and oxygen fugacity in olivine-hosted melt inclusions. Geology
758 40, 915–918. doi:10.1130/G32992.1.

759 Green, D.H., Hibberson, W.O., Kovacs, I., Rosenthal, A., 2010. Water and its influence on
760 the lithosphere-asthenosphere boundary. Nature 467, 448–451.

761 Guillou, H., Carracedo, J.C., Torrado, F.P., Badiola, E.R., 1996. K-Ar ages and mag-
762 netic stratigraphy of a hotspot-induced, fast grown oceanic island: El Hierro, Canary
763 Islands. Journal of Volcanology and Geothermal Research 73, 141–155. doi:10.1016/
764 0377-0273(96)00021-2.

765 Hansteen, T.H., Klügel, A., Schmincke, H.U., 1998. Multi-stage magma ascent beneath
766 the Canary Islands: evidence from fluid inclusions. Contributions to Mineralogy and
767 Petrology 132, 48–64. doi:10.1007/s004100050404.

768 Hartley, M.E., Maclennan, J., Edmonds, M., Thordarson, T., 2014. Reconstructing the
769 deep CO_2 degassing behaviour of large basaltic fissure eruptions. Earth and Planetary
770 Science Letters 393, 120–131. doi:10.1016/j.epsl.2014.02.031.

771 Hartley, M.E., Neave, D.A., Maclennan, J., Edmonds, M., Thordarson, T., 2015. Diffusive
772 over-hydration of olivine-hosted melt inclusions. Earth and Planetary Science Letters
773 425, 168–178. doi:10.1016/j.epsl.2015.06.008.

774 Herzberg, C., Asimow, P.D., 2008. Petrology of some oceanic island basalts:
775 PRIMELT2.XLS software for primary magma calculation. Geochemistry, Geophysics,
776 Geosystems 9, Q09001. doi:10.1029/2008GC002057.

777 Hirschmann, M.M., 2016. Constraints on the early delivery and fractionation of Earth's
778 major volatiles from C/H, C/N, and C/S ratios. American Mineralogist 101, 540–553.
779 doi:10.2138/am-2016-5452.

780 Hoernle, K.A.J., Schmincke, H.U., 1993. The role of partial melting in the 15-Ma geo-
781 chemical evolution of gran canaria: A blob model for the Canary hotspot. Journal of
782 Petrology 34, 599–626. doi:10.1093/petrology/34.3.599.

783 Hofmann, A.W., 1988. Chemical differentiation of the Earth: the relationship between
784 mantle, continental crust, and oceanic crust. Earth and Planetary Science Letters 90,
785 297–314. doi:10.1016/0012-821X(88)90132-X.

786 Hudgins, T.R., Mukasa, S.B., Simon, A.C., Moore, G., Barifaijo, E., 2015. Melt inclusion
787 evidence for CO_2-rich melts beneath the western branch of the East African Rift: impli-
788 cations for long-term storage of volatiles in the deep lithospheric mantle. Contributions
789 to Mineralogy and Petrology 169, 46. doi:10.1007/s00410-015-1140-9.

790 Kendrick, M.A., Jackson, M.G., Kent, A.J.R., Hauri, E.H., Wallace, P.J., Woodhead, J.,
791 2014. Contrasting behaviours of CO_2, S, H_2O and halogens (F, Cl, Br, and I) in enriched-
792 mantle melts from Pitcairn and Society seamounts. Chemical Geology 370, 69–81.
793 doi:10.1016/j.chemgeo.2014.01.019.

794 Klemme, S., O'Neill, H.S., 2000. The near-solidus transition from garnet lherzolite to
795 spinel lherzolite. Contributions to Mineralogy and Petrology 138, 237–248. doi:10.
796 1007/s004100050560.

797 Klügel, A., Hansteen, T.H., van den Bogaard, P., Strauss, H., Hauff, F., 2011. Holocene
798 fluid venting at an extinct Cretaceous seamount, Canary archipelago. Geology 39, 855–
799 858.

800 Klügel, A., Longpré, M.A., García-Cañada, L., Stix, J., 2015. Deep intrusions, lateral
801 magma transport and related uplift at ocean island volcanoes. Earth and Planetary Sci-
802 ence Letters 431, 140–149. doi:10.1016/j.epsl.2015.09.031.

803 Koleszar, A., Saal, A., Hauri, E., Nagle, A., Liang, Y., Kurz, M., 2009. The volatile
804 contents of the Galapagos plume; evidence for H_2O and F open system behavior in melt

inclusions. Earth and Planetary Science Letters 287, 442–452. doi:10.1016/j.epsl.2009.08.029.

Le Bas, M., Rex, D., Stillman, C., 1986. The early magmatic chronology of Fuerteventura, Canary Islands. Geological Magazine 123, 287–298. doi:10.1017/S0016756800034762.

Le Voyer, M., Asimow, P.D., Mosenfelder, J.L., Guan, Y., Wallace, P.J., Schiano, P., Stopler, E., Eiler, J., 2014. Zonation of H_2O and F concentrations around melt inclusions in olivines. Journal of Petrology 55, 685–707. doi:10.1093/petrology/egu003.

Longpré, M.A., 2009. Consequences of giant landslides on ocean island magmatism: volcanic and geochemical evolution of the Teno massif, Tenerife, and El Hierro Island (Canary Archipelago). Phd thesis. Trinity College, University of Dublin.

Longpré, M.A., Klügel, A., Diehl, A., Stix, J., 2014. Mixing in mantle magma reservoirs prior to and during the 2011–2012 eruption at El Hierro, Canary Islands. Geology 42, 315–318. doi:10.1130/G35165.1.

Longpré, M.A., Stix, J., Klügel, A., Shimizu, N., 2017. Mantle to surface degassing of carbon- and sulphur-rich alkaline magma at El Hierro, Canary Islands. Earth and Planetary Science Letters 460, 268–280. doi:10.1016/j.epsl.2016.11.043.

Lundstrom, C.C., Hoernle, K., Gill, J., 2003. U-series disequilibria in volcanic rocks from the Canary Islands: Plume versus lithospheric melting. Geochimica et Cosmochimica Acta 67, 4153–4177. doi:10.1016/S0016-7037(03)00308-9.

Lyubetskaya, T., Korenaga, J., 2007. Chemical composition of Earth's primitive mantle and its variance: 1. Method and results. Journal of Geophysical Research: Solid Earth 112. doi:10.1029/2005JB004223.

López, C., Blanco, M.J., Abella, R., Brenes, B., Cabrera Rodríguez, V.M., Casas, B., Domínguez Cerdeña, I., Felpeto, A., de Villalta, M.F., del Fresno, C., García, O., García-Arias, M.J., García-Cañada, L., Gomis Moreno, A., González-Alonso, E., Guzmán Pérez, J., Iribarren, I., López-Díaz, R., Luengo-Oroz, N., Meletlidis, S., Moreno, M., Moure, D., de Pablo, J.P., Rodero, C., Romero, E., Sainz-Maza, S., Sentre Domingo, M.A., Torres, P.A., Trigo, P., Villasante-Marcos, V., 2012. Monitoring the volcanic unrest of El Hierro (Canary Islands) before the onset of the 2011–2012 submarine eruption. Geophysical Research Letters 39, 1–7. doi:10.1029/2012GL051846.

Maclennan, J., 2017. Bubble formation and decrepitation control the CO_2 content of olivine-hosted melt inclusions. Geochemistry Geophysics Geosystems 18, 597–616. doi:10.1002/2016GC006633.

Marty, B., 2012. The origins and concentrations of water, carbon, nitrogen and noble gases on Earth. Earth and Planetary Science Letters 313-314, 56–66. doi:10.1016/j.epsl.2011.10.040.

Martí, J., Castro, A., Rodríguez, C., Costa, F., Carrasquilla, S., Pedreira, R., Bolos, X., 2013a. Correlation of magma evolution and geophysical monitoring during the 2011–2012 El Hierro (Canary Islands) submarine eruption. Journal of Petrology 54, 1349–1373. doi:10.1093/petrology/egt014.

Martí, J., Pinel, V., López, C., Geyer, A., Abella, R., Tárraga, M., Blanco, M.J., Castro, A., Rodríguez, C., 2013b. Causes and mechanisms of the 2011–2012 El Hierro (Canary Islands) submarine eruption. Journal of Geophysical Research: Solid Earth 118, 823–839. doi:10.1002/jgrb.50087.

McGee, L.E., Smith, I.E.M., Millet, M.A., Handley, H.K., Lindsay, J.M., 2013. Asthenospheric control of melting processes in a monogenetic basaltic system: a case study

852 of the Auckland Volcanic Field, New Zealand. Journal of Petrology 54, 2125–2153.
853 doi:10.1093/petrology/egt043.

854 McKenzie, D., O'Nions, R., 1991. Partial melt distributions from inversion of rare earth el-
855 ement concentrations. Journal of Petrology 32, 1021–1091. doi:10.1093/petrology/
856 32.5.1021.

857 Melián, G., Hernández, P.A., Padrón, E., Pérez, N.M., Barrancos, J., Padilla, G., Dio-
858 nis, S., Rodríguez, F., Calvo, D., Nolasco, D., 2014. Spatial and temporal variations
859 of diffuse CO_2 degassing at El Hierro volcanic system: Relation to the 2011–2012
860 submarine eruption. Journal of Geophysical Research: Solid Earth 119, 6976–6991.
861 doi:10.1002/2014JB011013.

862 Moore, L.R., Gazel, E., Tuohy, R., Lloyd, A.S., Esposito, R., Steele-MacInnis, M., Hauri,
863 E.H., Wallace, P.J., Plank, T., Bodnar, R.J., 2015. Bubbles matter: An assessment of the
864 contribution of vapor bubbles to melt inclusion volatile budgets. American Mineralogist
865 100, 806–823. doi:10.2138/am-2015-5036.

866 Moussallam, Y., Morizet, Y., Gaillard, F., 2016. H_2O–CO_2 solubility in low SiO_2-melts
867 and the unique mode of kimberlite degassing and emplacement. Earth and Planetary
868 Science Letters 447, 151–160. doi:10.1016/j.epsl.2016.04.037.

869 Moussallam, Y., Oppenheimer, C., Scaillet, B., Gaillard, F., Kyle, P., Peters, N., Hartley,
870 M., Berlo, K., Donovan, A., 2014. Tracking the changing oxidation state of Erebus
871 magmas, from mantle to surface, driven by magma ascent and degassing. Earth and
872 Planetary Science Letters 393, 200–209. doi:10.1016/j.epsl.2014.02.055.

873 Métrich, N., Rutherford, M.J., 1998. Low pressure crystallization paths of H_2O-saturated
874 basaltic-Hawaiitic melts from Mt Etna: Implications for open-system degassing of

basaltic volcanoes. Geochimica et Cosmochimica Acta 62, 1195–1205. doi:10.1016/S0016-7037(98)00048-9.

Métrich, N., Wallace, P.J., 2008. Volatile abundances in basaltic magmas and their degassing paths tracked by melt inclusions. Reviews in Mineralogy and Geochemistry 69, 363–402. doi:10.2138/rmg.2008.69.10.

Oppenheimer, C., Moretti, R., Kyle, P.R., Eschenbacher, A., Lowenstern, J.B., Hervig, R.L., Dunbar, N.W., 2011. Mantle to surface degassing of alkalic magmas at Erebus volcano, Antarctica. Earth and Planetary Science Letters 306, 261–271. doi:10.1016/j.epsl.2011.04.005.

Palme, H., O'Neill, H.S.C., 2003. Cosmochemical estimates of mantle composition. Treatise on Geochemistry 2, 1–38. doi:10.1016/B0-08-043751-6/02177-0.

Portnyagin, M., Almeev, R., Matveev, S., Holtz, F., 2008. Experimental evidence for rapid water exchange between melt inclusions in olivine and host magma. Earth and Planetary Science Letters 272, 541–552. doi:10.1016/j.epsl.2008.05.020.

Putirka, K.D., 2005. Mantle potential temperatures at Hawaii, Iceland, and the mid-ocean ridge system, as inferred from olivine phenocrysts: Evidence for thermally driven mantle plumes. Geochemistry, Geophysics, Geosystems 6. doi:10.1029/2005GC000915.

Putirka, K.D., 2008. Thermometers and barometers for volcanic systems. Reviews in Mineralogy and Geochemistry 69, 61–120. doi:10.2138/rmg.2008.69.3.

Pérez, N.M., Padilla, G.D., Padrón, E., Hernández, P.A., Melián, G.V., Barrancos, J., Dionis, S., Nolasco, D., Rodríguez, F., Calvo, D., Hernández, I., 2012. Precursory diffuse CO_2 and H_2S emission signatures of the 2011–2012 El Hierro submarine eruption, Canary Islands. Geophysical Research Letters 39, L16311. doi:10.1029/2012GL052410.

Rose-Koga, E., Koga, K., Moreira, M., Vlastelic, I., Jackson, M., Whitehouse, M.J., Shimizu, N., Habib, N., 2017. Geochemical systematics of Pb isotopes, fluorine, and sulfur in melt inclusions from São Miguel, Azores. Chemical Geology 458, 22–37. doi:10.1016/j.chemgeo.2017.03.024.

Rosenthal, A., Hauri, E.H., Hirschmann, M.M., 2015. Experimental determination of C, F, and H partitioning between mantle minerals and carbonated basalt, CO_2/Ba and CO_2/Nb systematics of partial melting, and the CO_2 contents of basaltic source regions. Earth and Planetary Science Letters 412, 77–87. doi:10.1016/j.epsl.2014.11.044.

Saal, A.E., Hauri, E.H., Langmuir, C.H., Perfit, M.R., 2002. Vapour undersaturation in primitive mid-ocean-ridge basalt and the volatile content of Earth's upper mantle. Nature 419, 451–455. doi:10.1038/nature01073.

Salters, V.J.M., Stracke, A., 2004. Composition of the depleted mantle. Geochemistry, Geophysics, Geosystems 5. doi:10.1029/2003GC000597.

Schmincke, H.U., 2004. Volcanism. volume 28. Springer Science & Business Media.

Shishkina, T.A., Botcharnikov, R.E., Holtz, F., Almeev, R.R., Portnyagin, M.V., 2010. Solubility of H_2O- and CO_2-bearing fluids in tholeiitic basalts at pressures up to 500MPa. Chemical Geology 277, 115–125.

Sigmarsson, O., Laporte, D., Carpentier, M., Devouard, B., Devidal, J.L., Marti, J., 2013. Formation of U-depleted rhyolite from a basanite at El Hierro, Canary Islands. Contributions to Mineralogy and Petrology 165, 601–622. doi:10.1007/s00410-012-0826-5.

Steele-Macinnis, M., Esposito, R., Bodnar, R.J., 2011. Thermodynamic model for the effect of post-entrapment crystallization on the H_2O–CO_2 systematics of vapor-

saturated, silicate melt inclusions. Journal of Petrology 52, 2461–2482. doi:10.1093/petrology/egr052.

Steele-MacInnis, M., Esposito, R., Moore, L.R., Hartley, M.E., 2017. Heterogeneously entrapped, vapor-rich melt inclusions record pre-eruptive magmatic volatile contents. Contributions to Mineralogy and Petrology 172, 18. doi:10.1007/s00410-017-1343-3.

Stroncik, N.A., Klügel, A., Hansteen, T.H., 2009. The magmatic plumbing system beneath El Hierro (Canary Islands): constraints from phenocrysts and naturally quenched basaltic glasses in submarine rocks. Contributions to Mineralogy and Petrology 157, 593–607. doi:10.1007/s00410-008-0354-5.

Troll, V.R., Klügel, A., Longpré, M., Burchardt, S., Deegan, F., Carracedo, J., Wiesmaier, S., Kueppers, U., Dahrén, B., Blythe, L., 2012. Floating stones off El Hierro, Canary Islands: xenoliths of pre-island sedimentary origin in the early products of the October 2011 eruption. Solid Earth 3, 97–110. doi:10.5194/se-3-97-2012.

Wallace, P.J., Kamenetsky, V.S., Cervantes, P., 2015. Melt inclusion CO_2 contents, pressures of olivine crystallization, and the problem of shrinkage bubbles. American Mineralogist 100, 787–794. doi:10.2138/am-2015-5029.

Wang, X., Chou, I.M., Hu, W., Burruss, R.C., Sun, Q., Song, Y., 2011. Raman spectroscopic measurements of CO_2 density: Experimental calibration with high-pressure optical cell (HPOC) and fused silica capillary capsule (FSCC) with application to fluid inclusion observations. Geochimica et Cosmochimica Acta 75, 4080–4093. doi:10.1016/j.gca.2011.04.028.

Weis, F.A., Skogby, H., Troll, V.R., Deegan, F.M., Dahren, B., 2015. Magmatic water

contents determined through clinopyroxene: Examples from the Western Canary Islands, Spain. Geochemistry, Geophysics, Geosystems 16, 2127–2146. doi:10.1002/2015GC005800.

Witham, F., Blundy, J., Kohn, S.C., Lesne, P., Dixon, J., Churakov, S.V., Botcharnikov, R., 2012. SolEx: A model for mixed COHSCl-volatile solubilities and exsolved gas compositions in basalt. Computers & Geosciences 45, 87–97. doi:10.1016/j.cageo.2011.09.021.

Figure1

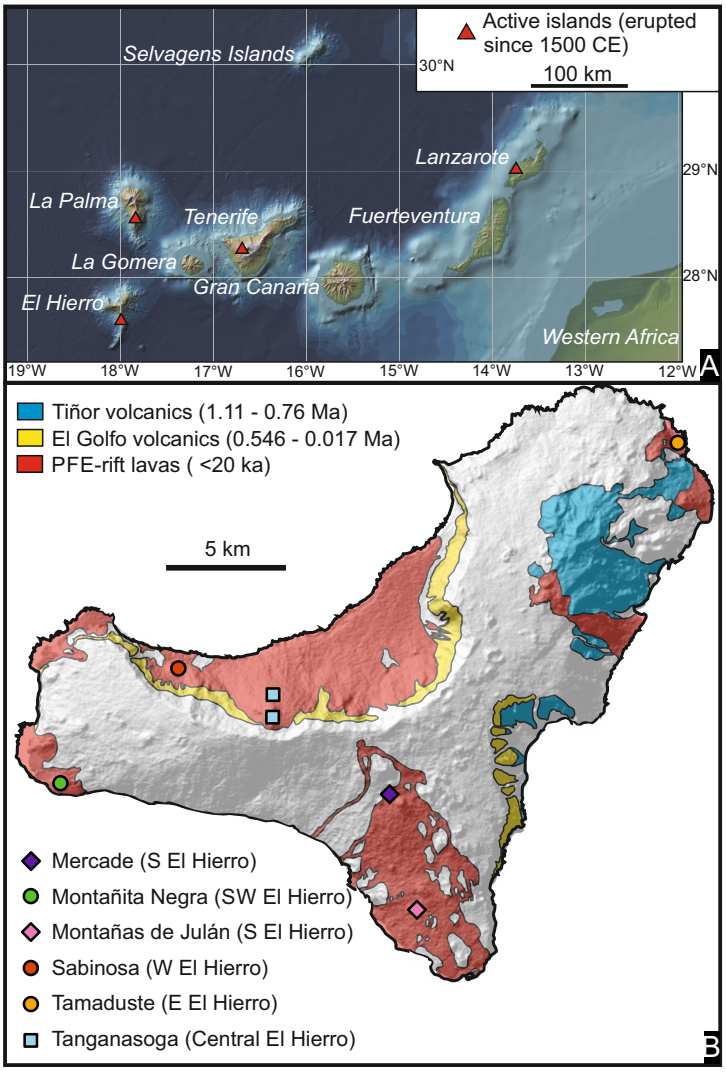
Active islands (erupted since 1500 CE)
100 km
Selvagens Islands
30°N
Lanzarote
29°N
La Palma
Tenerife
Fuerteventura
La Gomera
Gran Canaria
28°N
El Hierro
Western Africa
19°W
18°W
17°W
16°W
15°W
14°W
13°W
12°W
A
Tiñor volcanics (1.11 - 0.76 Ma)
El Golfo volcanics (0.546 - 0.017 Ma)
PFE-rift lavas (<20 ka)
5 km
Mercade (S El Hierro)
Montañita Negra (SW El Hierro)
Montañas de Julán (S El Hierro)
Sabinosa (W El Hierro)
Tamaduste (E El Hierro)
Tanganasoga (Central El Hierro)
B

Figure3

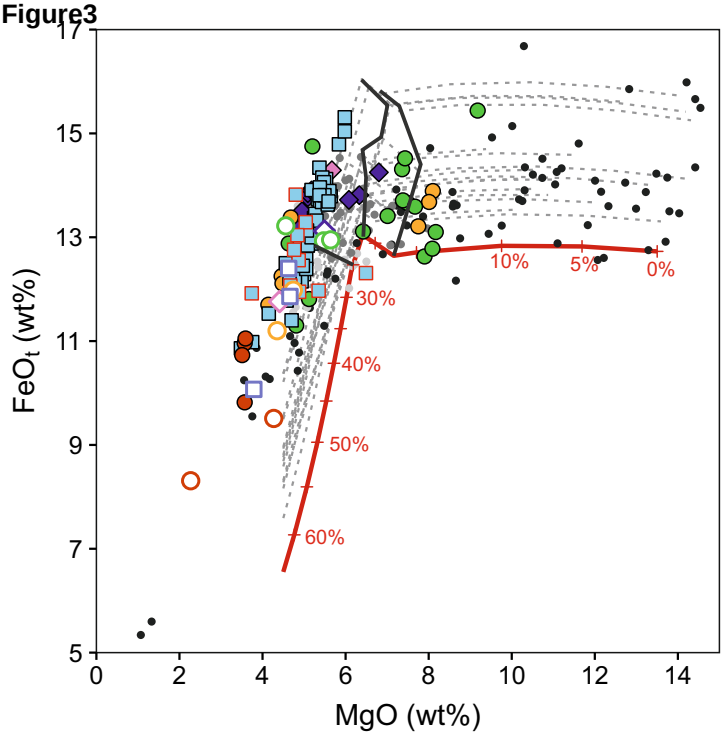
FeOt (wt%)
MgO (wt%)
10%
5%
0%
30%
40%
50%
60%

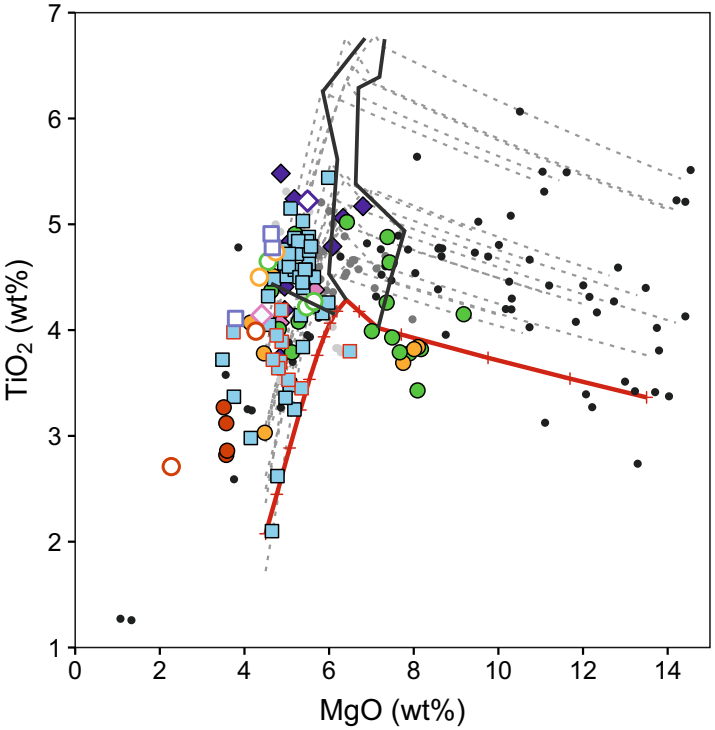
TiO2 (wt%)
MgO (wt%)

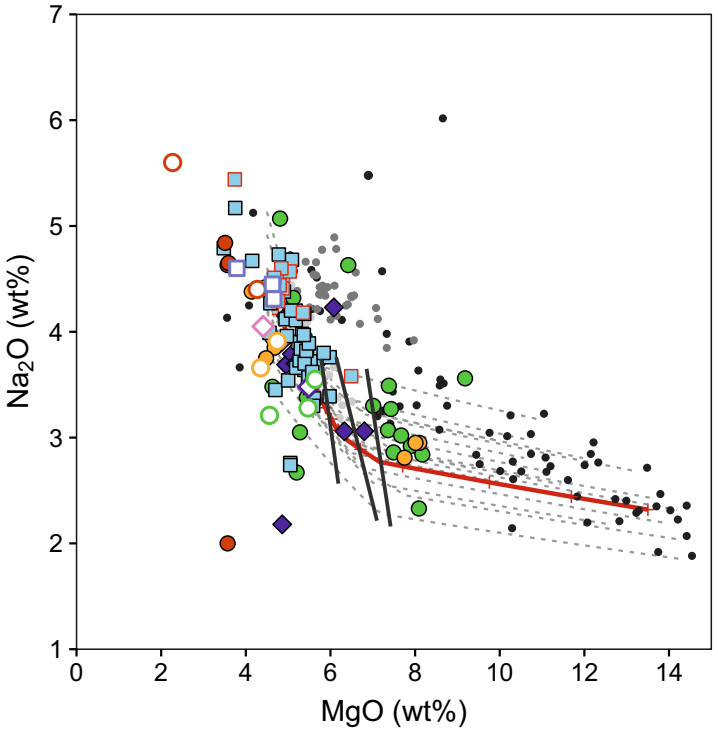
Na2O (wt%)
MgO (wt%)

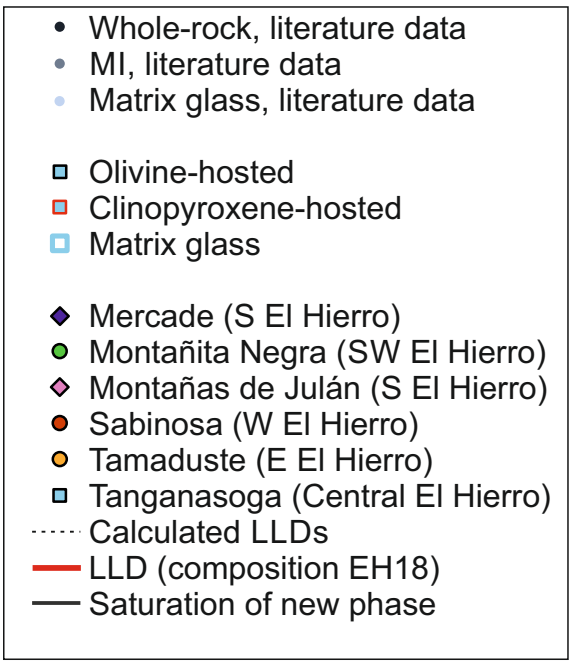
Whole-rock, literature data
MI, literature data
Matrix glass, literature data
Olivine-hosted
Clinopyroxene-hosted
Matrix glass
Mercade (S El Hierro)
Montañita Negra (SW El Hierro)
Montañas de Julán (S El Hierro)
Sabinosa (W El Hierro)
Tamaduste (E El Hierro)
Tanganasoga (Central El Hierro)
Calculated LLDs
LLD (composition EH18)
Saturation of new phase

Figure4

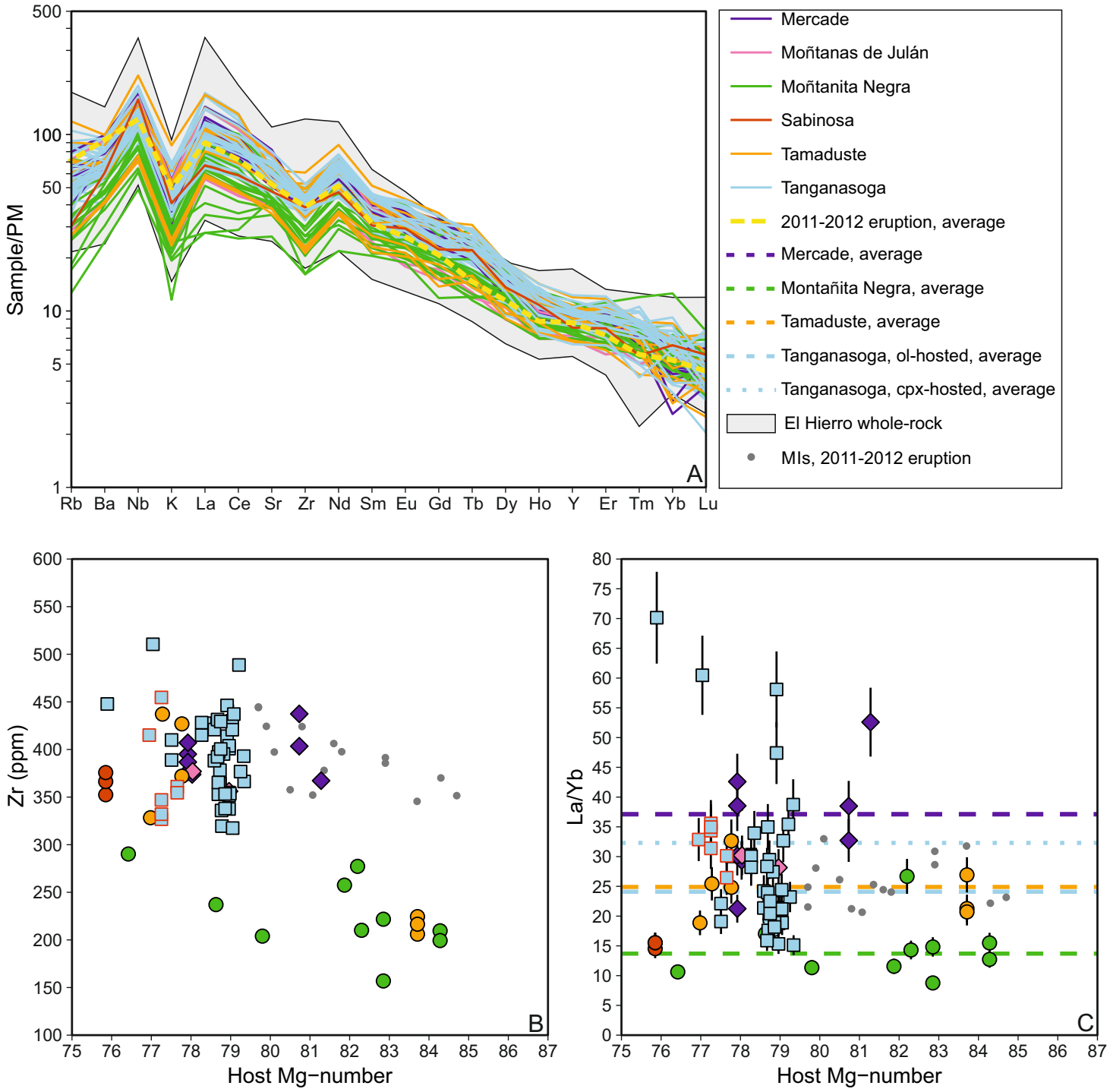
Sample/PM
500
100
50
10
5
1
Rb Ba Nb K La Ce Sr Zr Nd Sm Eu Gd Tb Dy Ho Y Er Tm Yb Lu
A
Mercade
Moñtanas de Julán
Moñtanita Negra
Sabinosa
Tamaduste
Tanganasoga
2011-2012 eruption, average
Mercade, average
Montañita Negra, average
Tamaduste, average
Tanganasoga, ol-hosted, average
Tanganasoga, cpx-hosted, average
El Hierro whole-rock
MIs, 2011-2012 eruption
Zr (ppm)
600
550
500
450
400
350
300
250
200
150
100
75 76 77 78 79 80 81 82 83 84 85 86 87
Host Mg−number
B
La/Yb
80
75
70
65
60
55
50
45
40
35
30
25
20
15
10
5
0
75 76 77 78 79 80 81 82 83 84 85 86 87
Host Mg−number
C

Figure5

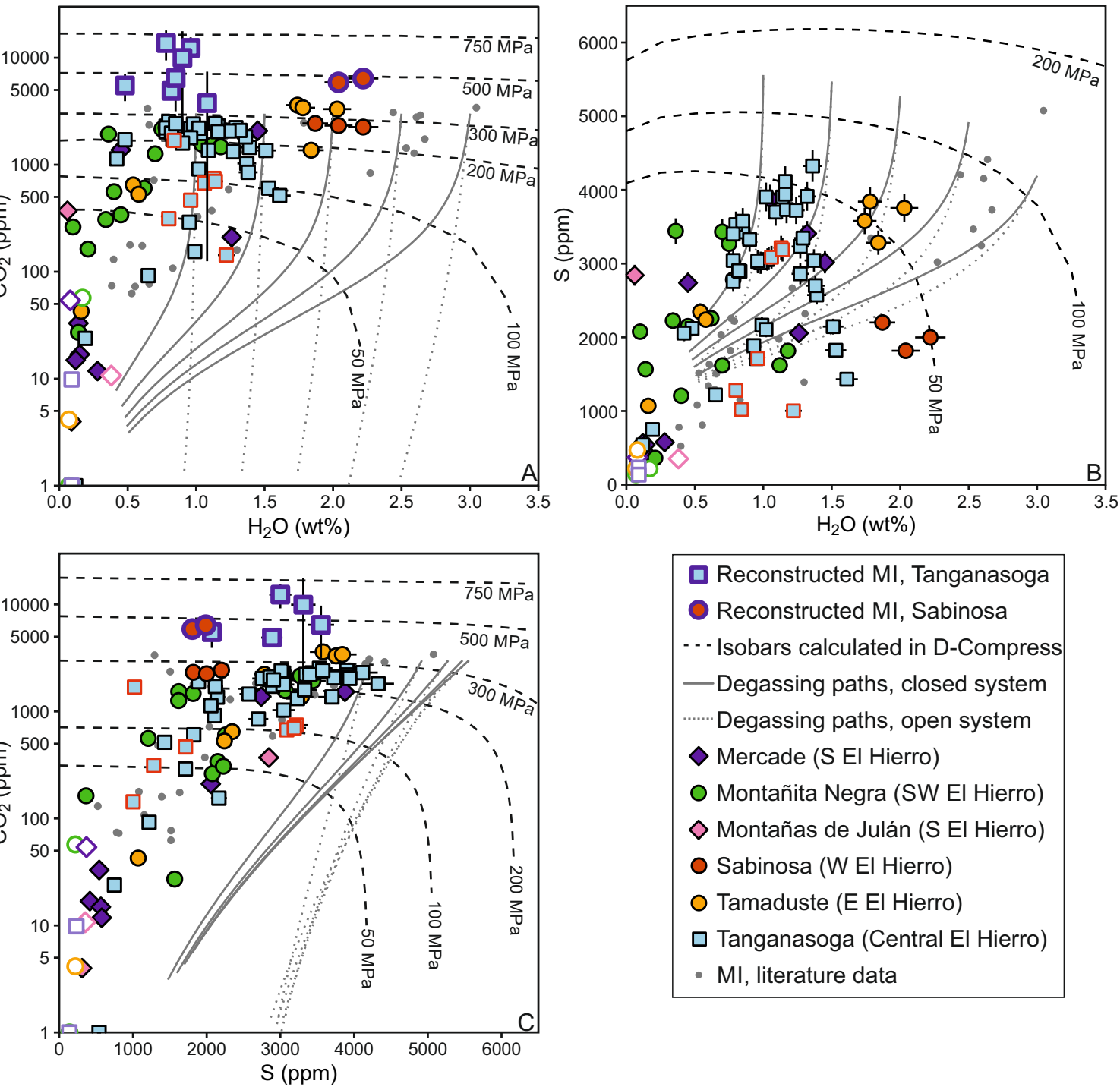
750 MPa
500 MPa
300 MPa
200 MPa
100 MPa
50 MPa
A
B
C
H2O (wt%)
S (ppm)
Reconstructed MI, Tanganasoga
Reconstructed MI, Sabinosa
Isobars calculated in D-Compress
Degassing paths, closed system
Degassing paths, open system
Mercade (S El Hierro)
Montañita Negra (SW El Hierro)
Montañas de Julán (S El Hierro)
Sabinosa (W El Hierro)
Tamaduste (E El Hierro)
Tanganasoga (Central El Hierro)
MI, literature data

Figure6

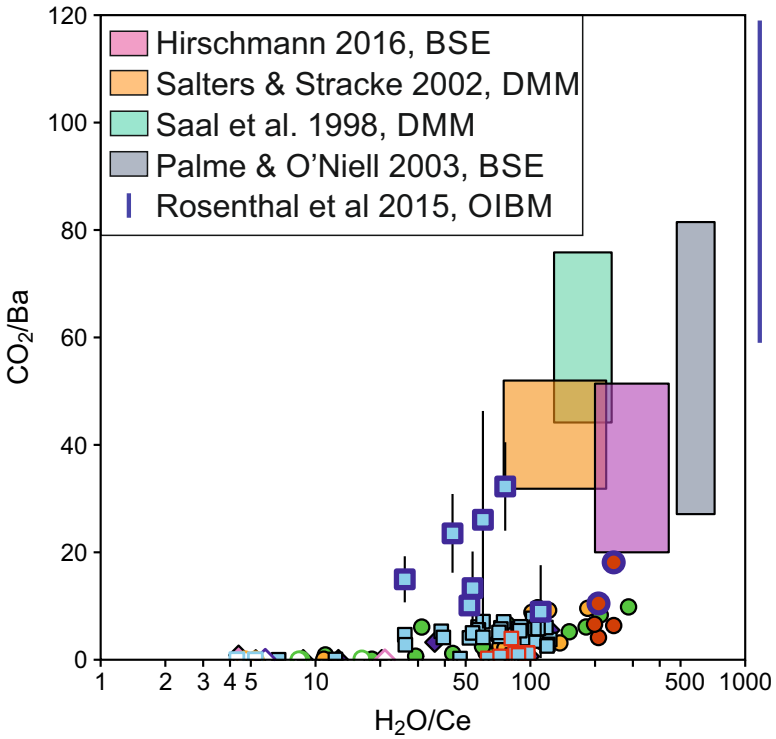
Hirschmann 2016, BSE
Salters & Stracke 2002, DMM
Saal et al. 1998, DMM
Palme & O'Niell 2003, BSE
Rosenthal et al 2015, OIBM
CO2/Ba
H2O/Ce
120
100
80
60
40
20
0
1
2
3
4
5
10
50
100
500
1000

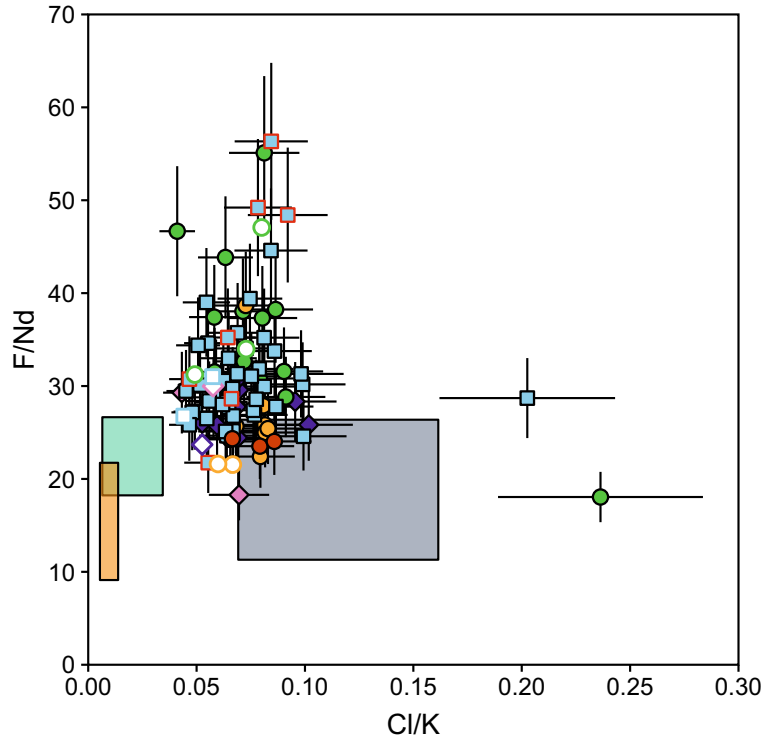
F/Nd
Cl/K
70
60
50
40
30
20
10
0
0.00
0.05
0.10
0.15
0.20
0.25
0.30

Figure7

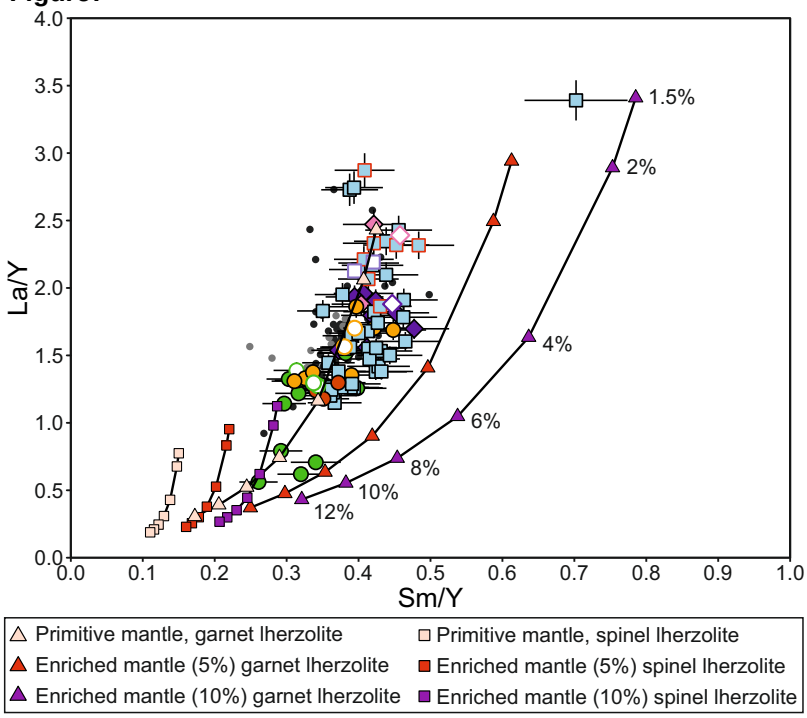

△ Primitive mantle, garnet lherzolite
□ Primitive mantle, spinel lherzolite
▲ Enriched mantle (5%) garnet lherzolite
■ Enriched mantle (5%) spinel lherzolite
▲ Enriched mantle (10%) garnet lherzolite
■ Enriched mantle (10%) spinel lherzolite

Figure8

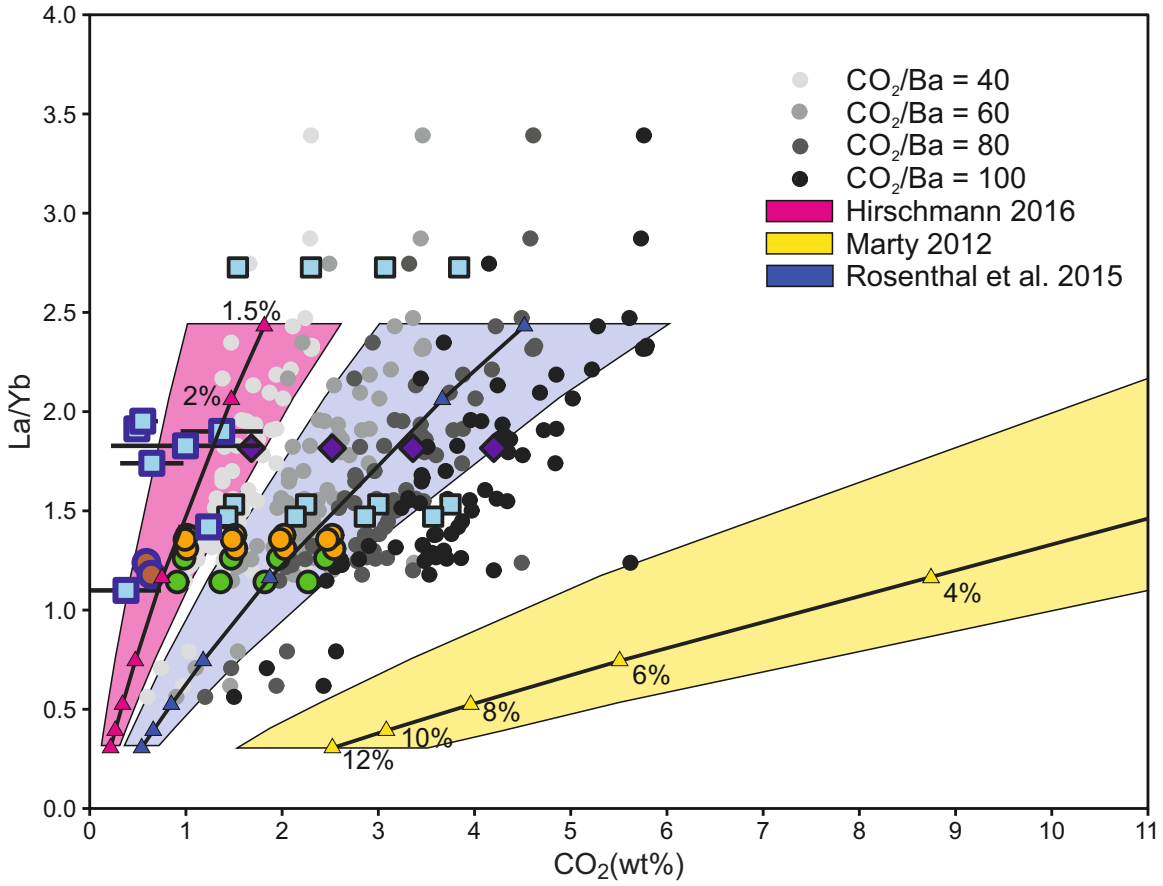
4.0
3.5
3.0
2.5
2.0
1.5
1.0
0.5
0.0
La/Yb
0
1
2
3
4
5
6
7
8
9
10
11
CO2(wt%)
CO2/Ba = 40
CO2/Ba = 60
CO2/Ba = 80
CO2/Ba = 100
Hirschmann 2016
Marty 2012
Rosenthal et al. 2015
1.5%
2%
4%
6%
8%
10%
12%

Figure9

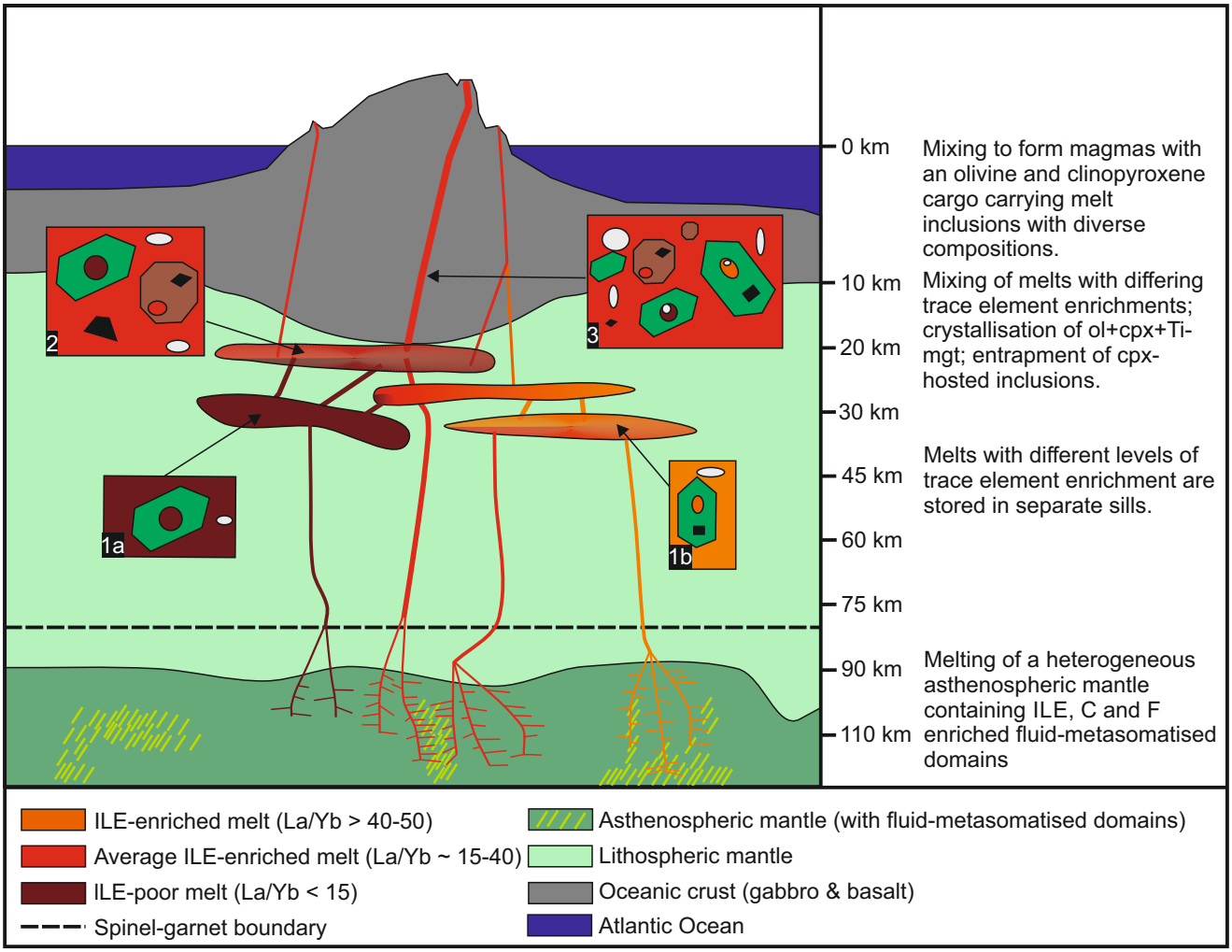
0 km
10 km
20 km
30 km
45 km
60 km
75 km
90 km
110 km
Mixing to form magmas with an olivine and clinopyroxene cargo carrying melt inclusions with diverse compositions.
Mixing of melts with differing trace element enrichments; crystallisation of ol+cpx+Ti-mgt; entrapment of cpx-hosted inclusions.
Melts with different levels of trace element enrichment are stored in separate sills.
Melting of a heterogeneous asthenospheric mantle containing ILE, C and F enriched fluid-metasomatised domains
1a
1b
2
3
ILE-enriched melt (La/Yb > 40-50)
Average ILE-enriched melt (La/Yb ~ 15-40)
ILE-poor melt (La/Yb < 15)
Spinel-garnet boundary
Asthenospheric mantle (with fluid-metasomatised domains)
Lithospheric mantle
Oceanic crust (gabbro & basalt)
Atlantic Ocean